1-1-1971

Reactivity measurements based on the pulsed neutron technique

George William Hannaman
Iowa State University

Reactivity measurements based on the pulsed neutron technique

by

George William Hannaman, Jr.

A Thesis Submitted to the
Graduate Faculty in Partial Fulfillment of
The Requirements for the Degree of

MASTER OF SCIENCE

Major Subject: Nuclear Engineering

Iowa State University
Ames, Iowa

1971

TABLE OF CONTENTS

I. INTRODUCTION

Since 1956, the pulsed-neutron technique has been used to measure reactivity [27]. Several investigators developed techniques to convert the quantities observed in a pulsed-neutron experiment such as the fundamental decay constant, delayed neutron contribution, and the prompt neutron response, into the parameter of reactivity. These methods have become refined to the point that the measurements combined with calculational techniques can be used to convert the measured quantities into accurate values of reactivity. Preskitt et al. [23] point out that most reactor designers use the parameter of reactivity since it relates to the neutron multiplication of the system. Further, reactivity cannot be uniquely determined entirely from observable quantities except by the measurement of spatial averages, and for other cases some quantities based entirely on calculation must be provided. Therefore, to provide a check of the calculations needed to determine reactivity, the focal point should be a measurable quantity.

The work presented in this thesis deals with the use of the pulsed-neutron technique to determine reactivity and control rod worths in the UTR-10 coupled core reactor. A pulsed-neutron experiment consists of subjecting the reactor to a burst of neutrons and observing the subsequent time behavior of the neutron flux. During the course of this work it was found that the measurable quantities associated with this time behavior have variations as a result of physical changes in the reactor.

With proper development, this behavior might be used to solve some of the problems encountered in the handling of fissile materials. Kratzer [17] points out that since the level of atomic power production is increasing, the volume of fissile material in circulation is also increasing. He suggests that experimental methods of measuring the amounts of uranium and plutonium during various stages of the fuel cycle are needed. As a result of this study, it is felt that the pulsed-neutron technique could be used to measure some of the properties of reactor fuel elements and assemblies of such elements.

II. LITERATURE SURVEY

Since the primary objective of this study was to measure the reactivity of the UTR-10 with various control rod positions, the literature search was employed to review the theory and experimental procedures used by other investigators who have made reactivity measurements in multiplying media. In addition to the reactivity measurements, there was interest in the determination of the optimal procedures to be utilized in future experiments.

The pulsed neutron technique has been used successfully for several years to measure reactivity. The different treatments of the data all depend on the prompt fundamental-mode decay constant [11, 12, 25, 26]. This decay constant is generally designated as α_0. When a detector is placed in a pulsed assembly, the results observed on a multichannel analyzer have the basic characteristics shown in Figure 1. From time zero to time T_1 the detector response is strongly influenced by the higher prompt harmonics which decay much faster than the prompt fundamental mode. The decay from T_1 to T_2 is characterized by the prompt fundamental mode alone which, if observed on a semi-log scale, appears as a straight line. After T_2 the detector response is determined by the decay of the delayed neutron precursors. The prompt neutron decay is much faster than the delayed neutron decay so that the delayed neutron counting rate can usually be considered as a constant for the conditions of a pulsed neutron experiment. This constant can be subtracted from the total response to obtain the prompt neutron response to the injected burst of neutrons.

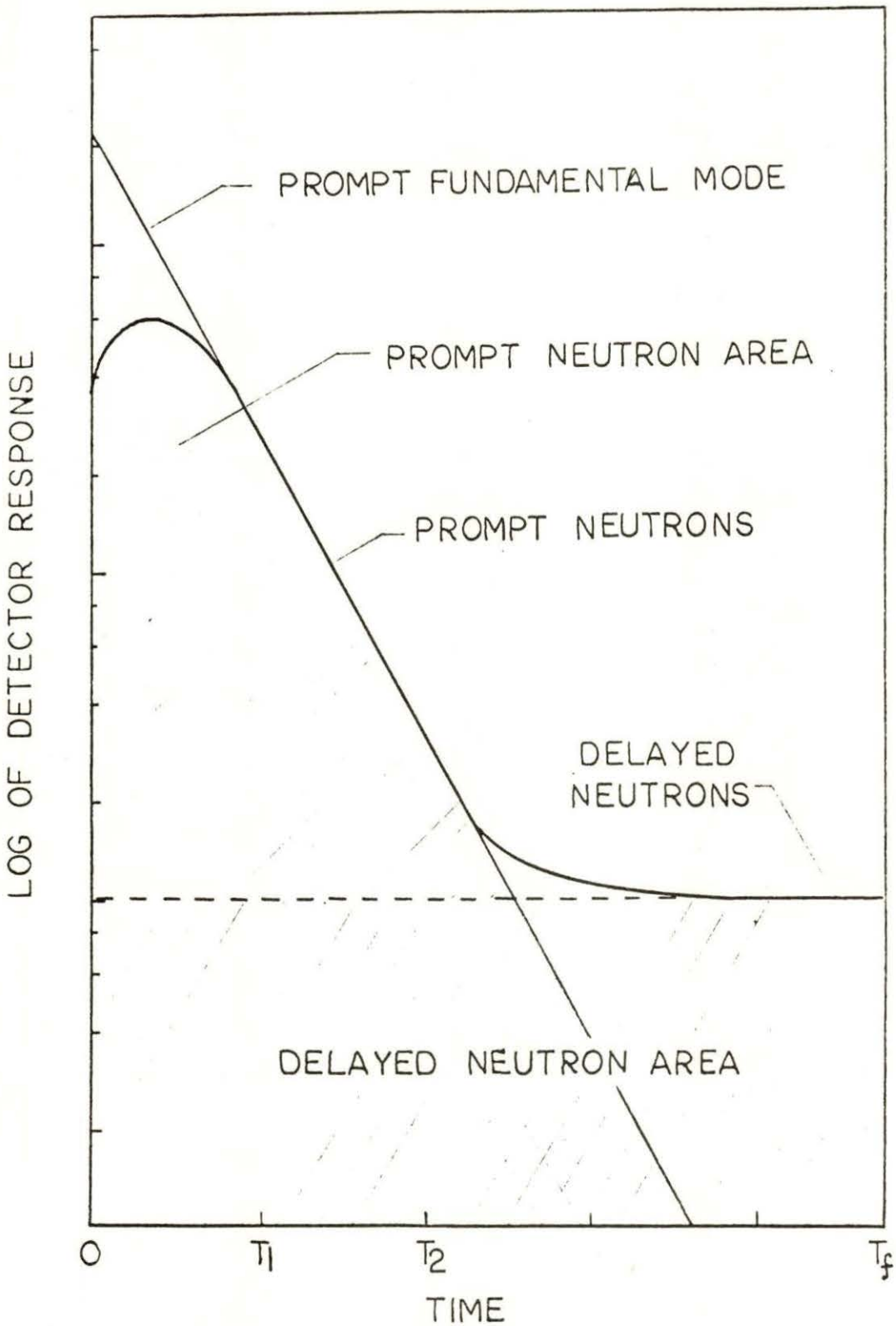

Figure 1. Ideal detector response to a pulsed neutron source.

The first investigator to measure reactivity with the pulsed-neutron technique was Sjöstrand [26]. He developed the area-ratio method, and obtained the negative reactivity from the ratio of the area of the prompt neutrons to the area of the delayed neutrons as shown in Figure 1. The results of this method are shadowed by the strong influence of higher spatial harmonics.

Simmons and King [25] pointed out that at delayed critical the reactivity is zero. Thus, if a calibration measurement of α_0 is made at delayed critical, the reactivity can be found for any subsequently measured α_0. This method assumes that β/ℓ is constant over the reactivity range of interest. This assumption does not always hold as pointed out by Garelis and Russell [11], and a correction factor to the prompt generation time[a] is needed. This correction is quite difficult to make in the Simmons-King method according to Becker and Quisenberry [2]. Another problem is the inconvenient necessity of a measurement of α_0 at delayed critical. This measurement is somewhat difficult to obtain because of the power level drift. Since each pulse will cause a small increase in the power level, several control rod adjustments may be needed to obtain sufficient counts for a determination of α_0.

In an effort to eliminate the problems associated with the method of Simmons and King, two subsequent investigators developed methods that do not require a measurement at delayed critical.

---

[a] The prompt generation time Λ, is related to the lifetime ℓ, by $\Lambda = \ell/k$.

Gozani's [12] method is a significant improvement over Sjöstrand's in that it eliminates the prompt higher harmonics by waiting until they have decayed before counting the prompt neutrons. The prompt neutron time behavior is then extrapolated back to zero time. The negative reactivity can be determined by taking the ratio of the prompt fundamental area to the delayed neutron area. Figure 1 shows the extrapolated area which is taken to T_f. A small correction factor is needed for the admixture of prompt and delayed eigenvalues.

Another method of analysis developed by Garelis and Russell [11], which is similar to Gozani's method, modified the Simmons-King technique by introducing a new parameter to replace the delayed critical decay constant. This parameter is $k\beta/\ell$. The application of this method is independent of higher harmonics and the constant generation time assumption. The development of their theory is based on a bare reactor containing monoenergic neutrons. The pulsed source is considered to be a repetitively pulsed delta function. Gozani [12] has shown that when a square pulse is used the same type of source term results if the pulse width is small. Even though these assumptions are not met in most assemblies, the experimental use of this method has given good results [8, 10, 16, 19].

Becker and Quisenberry [2], also Preskitt et al. [23], discuss the problems associated with the spatial dependence of pulsed neutron reactivity measurements. Becker and Quisenberry indicate that an important consideration for reflected systems is the correct placement of the neutron detector. The reason for this comes from the difference in the prompt and delayed modal shapes in a reflected

system. In their study, the smallest corrections of a few per cent appeared in the fuel region about half way between the reactor centerline and inner reflector surface.

Preskitt et al. [23] developed the concept of kinetic distortion which is used as a spatial correction to the reactivity measurement. Sophisticated computer codes are needed to accurately calculate this factor. They also show this factor tends to be the ratio of the fundamental delayed and prompt modes. In general, the kinetic distortion increases as the reactor becomes more subcritical. This is especially significant in the low absorption reflector region.

In an excellent study at the University of Florida, Ohanian and Diaz [22] measured spatial effects of the different parameters associated with the Garelis-Russell technique. The most significant results are; first, the variation in $k\beta/\ell$ with pulse width. Although α_0 was approximately constant, $k\beta/\ell$ varied inversely as the pulse width. Secondly, there was a variation of both α_0 and $k\beta/\ell$ with distance from the source, α_0 decreased, but $k\beta/\ell$ increased. The measured parameters from this experiment appeared to approach an equilibrium value for large distance between the source and detector. This distance should be large enough to insure that the detector is in the asymptotic region, where α_0 is observed.

The application of the pulsing technique has been used on the UTR-10 by Moen [21] to obtain the frequency response experimentally and to compare this with various reactor models. Betancourt [3], who developed one of the models, calculated the distributions of the delayed and thermal fluxes. The model shows the relative magnitudes as

a function of position for several modes. This study was carried out for the critical reactor, but a similar study could be made for subcritical states of the reactor. This information could then be used to make a reactivity correction for kinetic distortion. The shapes of both the prompt thermal and delayed modes are approximately the same, as calculated by Betancourt's model at critical.

For the studies made in this thesis, the Sjöstrand, the Garelis-Russell, and Gozani methods of data analysis will be used to determine the system reactivity.

Table I. A summary of the theoretical models used to compute reactivity from experimental pulsed data.

A. PULSED NEUTRON EXPERIMENTS

1. Simmons-King

$$-\rho(\$) = \frac{\alpha_0}{\alpha_c} - 1$$

B. MODIFIED PULSED NEUTRON EXPERIMENTS

1. Sjöstrand

$$-\rho(\$) = \frac{\text{prompt neutron area}}{\text{delayed neutron area}}$$

2. Gozani

$$-\rho(\$) = \frac{\text{extrapolated prompt fundamental mode area}}{\text{delayed neutron area}}$$

3. Garelis-Russell

$$-\rho(\$) = \frac{\alpha_0}{k\beta/\ell} - 1$$

where $k\beta/\ell$ satisfies

$$\int_0^\infty N_p(t) e^{(k\beta/\ell)t} dt = \int_0^\infty N_p(t) dt + \int_0^\infty N_d(t) dt$$

III. THEORY

Consider a pulsed neutron experiment where the data show the characteristics of Figure 1. The theory must relate the observable quantities to the desired reactor parameters. The relationship between α_0, the observable decay constant, and reactivity, the desired reactor parameter, can be seen by application of the reactor kinetic equation [15]

$$\frac{dn}{dt} = \frac{(k - 1)/k - \beta}{\Lambda} n + \sum_i \lambda_i C_i \ . \tag{1}$$

Here n is the neutron density as a function of time, Λ is the prompt generation time, β is the fraction of delayed neutrons[a], λ_i is the decay constant for the i^{th} group of delayed neutrons, and C_i is the concentration of the i^{th} precursor. For this development, consider prompt neutron decay and neglect the delayed neutrons since their contribution is considered a constant. Then, from the basic definition of the decay constant, which is a fractional change in the neutron density for a corresponding change in time, it follows that

$$\alpha_0 \equiv \frac{\Delta n}{n} \frac{1}{\Delta T} = \frac{1}{n} \frac{dn}{dt} = \frac{(k - 1)/k - \beta}{\Lambda} \ . \tag{2}$$

The commonly used unit of reactivity is the dollar, and is defined as $(k - 1)/k\beta$. Substituting this back into Eq. (2) yields

$$\alpha_0 = \frac{\beta}{\Lambda} (\rho(\$) - 1) = \frac{k\beta}{\ell} (\rho(\$) - 1). \tag{3}$$

---

[a] In D_2O or Be systems, the production of photoneutrons may be included in the delayed fraction.

Thus the measured fundamental-mode decay constant is directly proportional to the reactivity in dollar units.

Solving Eq. (3) for reactivity, and noting that at delayed critical $\alpha_{DC} = \beta/\ell$ then,

$$\rho(\$) = \frac{\alpha_0}{\alpha_{DC}} - 1 \tag{4}$$

which is the Simmons and King experimental formulation. Reactivity can be found from the two separate measurements of α_0 and α_{DC}.

The Garelis-Russell technique is used to solve for this parameter with the following equation

$$\int_0^\infty N_p \exp[(\alpha_{G-R} t)]dt = \int_0^\infty N_p dt + N_d/R. \tag{5}$$

Here N_p represents the prompt neutron contribution as a function of time, N_d is the delayed neutron contribution which is assumed constant, and R is the effective pulse rate as determined by the actual pulse rate and the analyzer sweeps per burst [9]. The parameter α_{G-R} is $k\beta/\ell$ and the method is sometimes referred to as the "$k\beta/\ell$ method".

The following experimental conditions should be met for proper application of this method. First, the effective pulsing rate R should be much greater than λ where λ is the decay constant of the shortest lived precursor. Second, R should be much less than α_0, the prompt fundamental decay constant. Third, the number of pulses must be large enough so that $\exp(-ma_{sn}/R) \ll \exp(-a_{sn}/R)$ where $m + 1$ is the number of pulses and a_{sn} are the roots of the inhour equation. Fourth, the prompt root must dominate the neutron

decay. When the previous conditions are met, the reactivity of the system can be found by

$$\rho(\$) = \frac{\alpha_0}{k\beta/\ell} - 1. \tag{6}$$

Gozani's extrapolated technique solves for the prompt fundamental area and the delayed neutron area with the following formula

$$\rho(\$) = \frac{N_p(0)(1 - e^{\alpha_0 T})}{TN_d\,\alpha_0} C_d \ . \tag{7}$$

In Eq. (7), $N_p(0)$ is the zero time extrapolated value of the prompt fundamental mode, T is the period of pulsing, and Nd is the delayed neutron constant background. C_d is the correction factor for differences in prompt and delayed eigenvalues, and α_0 is the prompt persisting decay constant. The prompt area can be represented by $N_p(0)(1 - e^{\alpha_0 T})/\alpha_0$, and the delayed area by $T \times N_d$. This method is generally called the extrapolated area-ratio method.

These methods are developed in Appendices A and B.

IV. EXPERIMENTAL PROCEDURE

The experiment was performed by injecting bursts of 14.3 MeV neutrons into the reactor and the response was measured with the aid of BF_3 filled detectors located in the core tanks. The time response was recorded in a multichannel analyzer.

A. Equipment

The measurements of reactivity were performed on the UTR-10 which is a coupled core Argonaut type reactor. Figure 2 shows a view of the exposed reactor core. The south core tank is in the upper portion of the picture. The number one safety rod is removed from the core and the empty slot shows its location when the reactor is in use. The worth of both safety rod number one and number two was measured. The number two safety rod is located in the upper left of Figure 2, while the number one rod and its mechanical components are seen in Figure 3. The square control element is made of boral and measures 7 in. x 7 in. x 1/8 in. Both safety rods have the same dimensions. Reactivity changes in the reactor are accomplished by movement of the control rods. The rod positions during the experiment were both fully inserted, safety rod number one removed, and both rods removed. Measurements were taken from detectors placed at the centerline of the core tanks as shown in Figure 4. The reason for placing the detectors in this position was to minimize the kinetic distortion factor. A monitor detector was placed in the central stringer position to obtain a normalizing flux which could be used in a flux shape analysis. The reactor was operated at a temperature of $92.0 \pm 0.5^{\circ}F$.

Figure 2. Top view of the UTR-10 core area with safety rod number one removed.

Figure 3. Safety rod number one and its mechanical assembly.

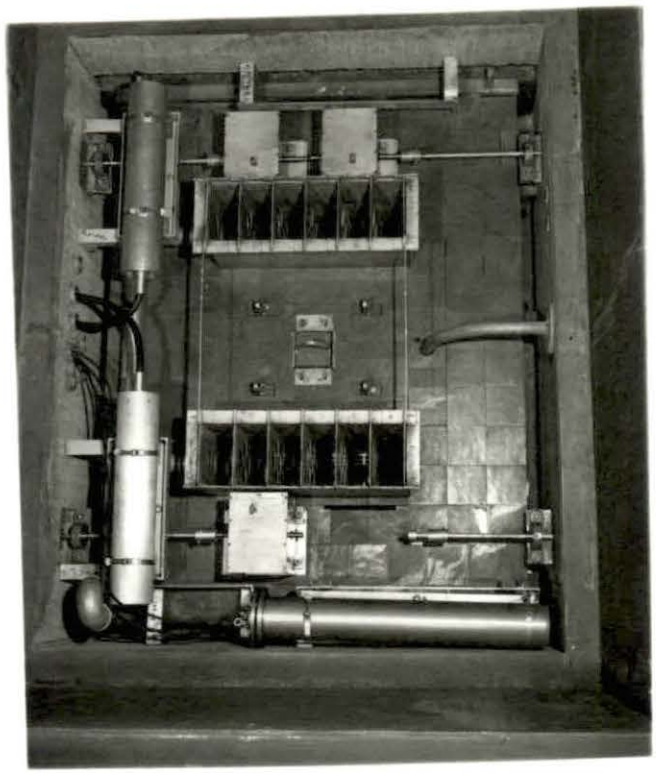

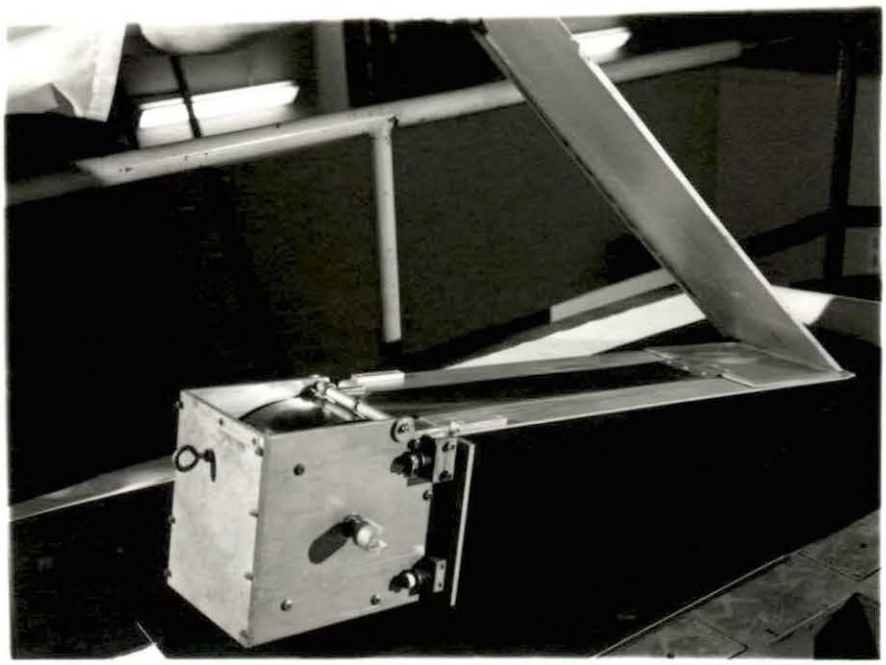

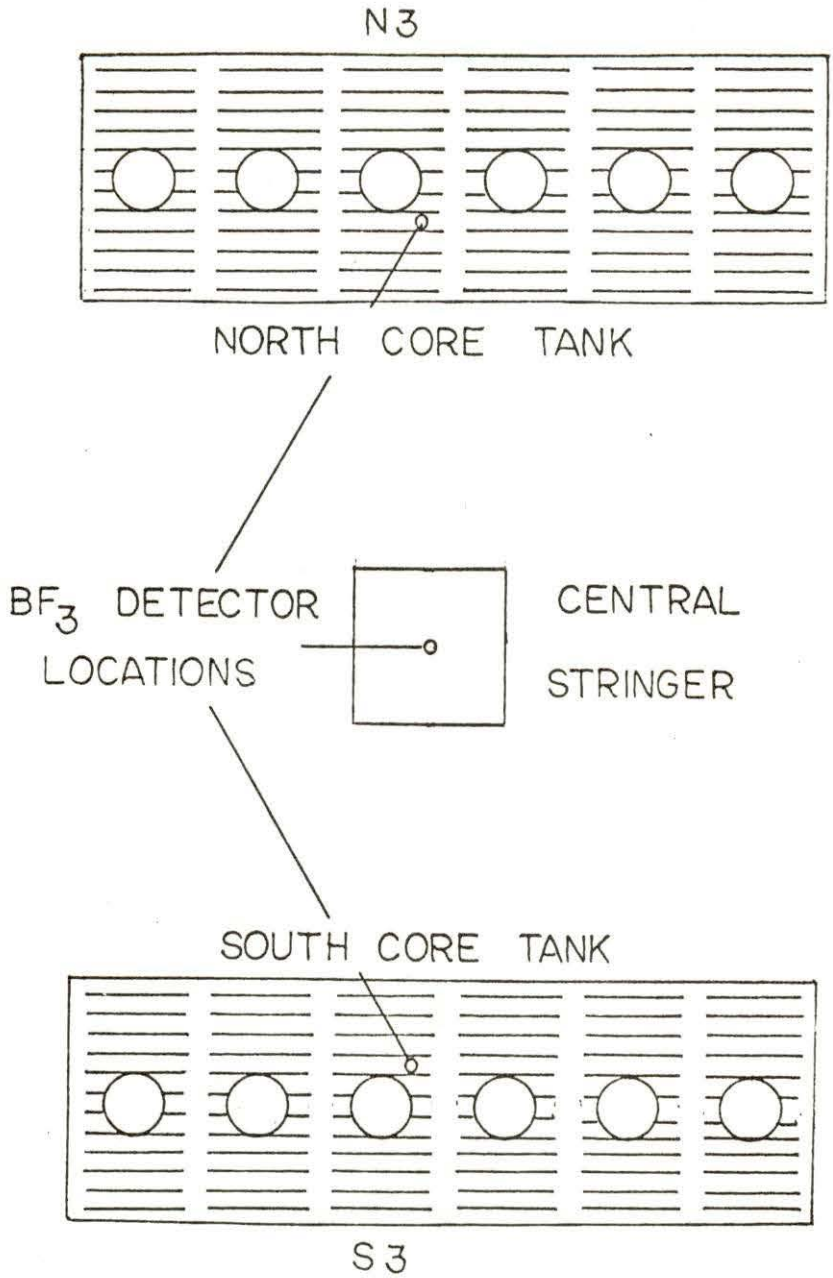

Figure 4. Detector positions during thermal column pulsing.

This temperature change resulted in less than a one per cent change in reactivity during the experiment [1].

The burst of neutrons was produced with a Kaman nuclear model A-800 neutron generator. Figure 6 shows the neutron generator and its control console near the entrance of the thermal column. This model produces neutrons by the $^{2}H + {}^{3}H \rightarrow {}^{4}He + n + 17.6$ MeV reaction. The neutron generator operates in the following manner [13]. Deuterium gas is produced by electrically heating a tungsten element around which is wrapped a coil of deuterium impregnated zirconium wire. The rate of gas evolution is controlled by the variation in the element temperature. The electrons are removed from the gas in a Penning ion gage. Then the deuterium ions are accelerated toward the tritium target with a 120kV pulse. The unit is insulated with SF_6 gas to protect it from insulation breakdown. The deuterium ions bombard the tritium atoms in the target, which is located about 7-3/8 in. from the end of the accelerator assembly. This produces an isotropic yield of more than 10^7 neutrons in about 3 μsec, as shown in Figure 7. The pulse rate of the neutron generator is limited by temperature considerations to 5 pulses/sec for continuous operation. As the neutrons progress through the assembly, their energy is reduced to thermal energy. The neutrons then interact with uranium causing fissions, and this total neutron response is measured with the detectors. The detectors used were N.C. Wood model G-3-20 BF_3 Neutron Detectors, 3/8 in. diameter, and 20 in. long. The detection of a neutron takes place because of the following reaction [24, pp. 313-317], $^{10}B + n \rightarrow {}^{7}Li + {}^{4}He + 2.78$ MeV. The cross section for this

Figure 5. Electronic equipment used in storing data.

Figure 6. Kaman neutron generator model A-800 and its control console.

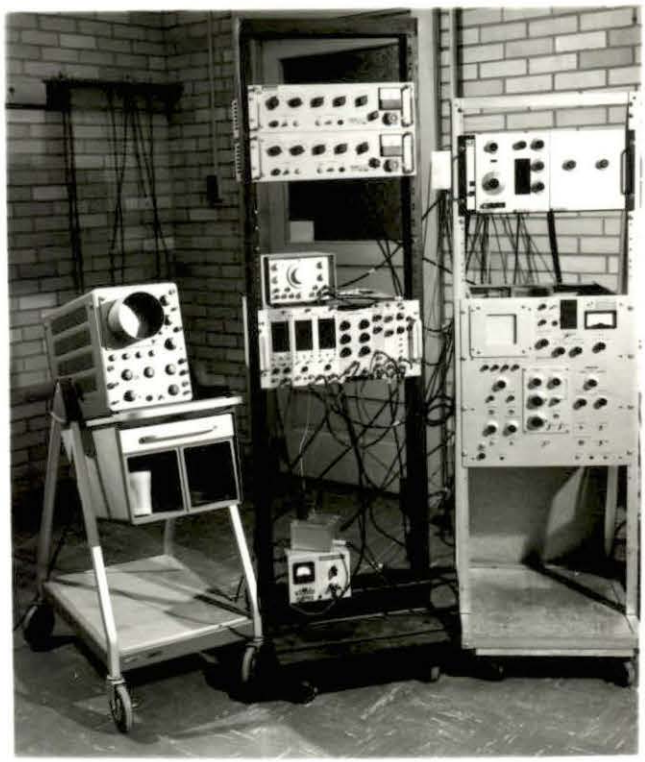

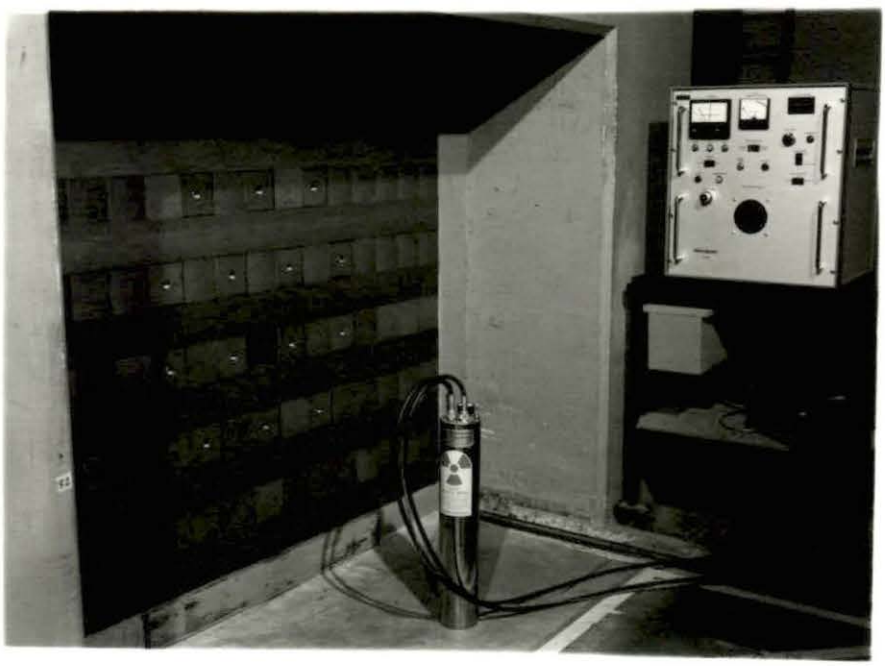

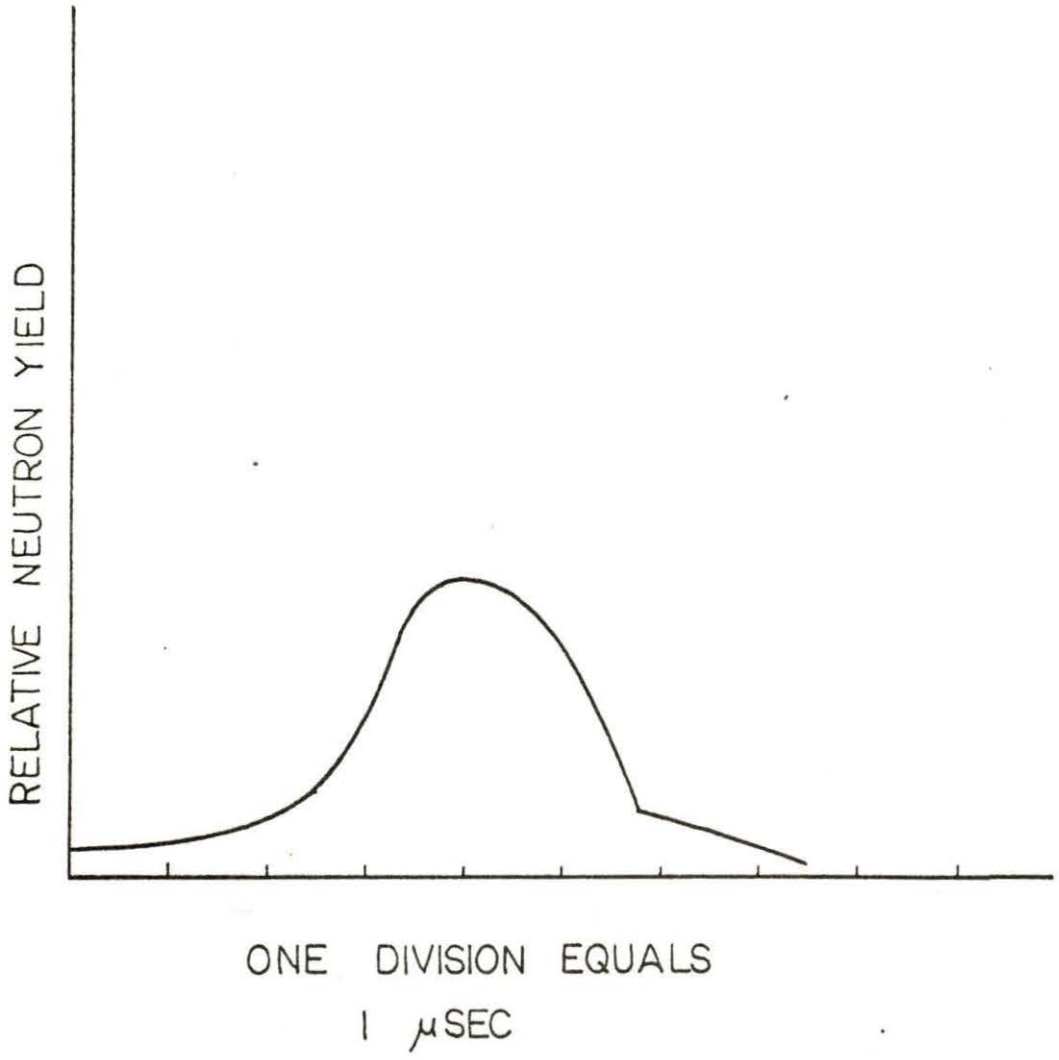

Figure 7. Neutron yield from the generator as a function of time [13].

reaction is 3840 $\pm$ 11 b at a neutron velocity of 2200 m/sec. The ion pairs produced by the charged particles are collected with the aid of an electric field within the detector. The detectors have a flat response from about 1100 v to 1400 v, where an increase in the count rate begins. The Fluke high voltage supply was set for 1300 volts during the experimental runs. A check on the energy response of the detector revealed that less than 5 per cent of the counts recorded were caused by epicadmium neutrons.

A block diagram of the electronics system can be seen in Figure 8, and Figure 5 shows the actual equipment used. The pre-amplifier converts the detector output of charge into a voltage signal. The voltage signal is amplified by the ORTEC 410 linear amplifier. The detector response to a neutron produces about the same amount of charge each time. This charge is greater than that produced by gamma rays, therefore a discriminator is used to separate the neutron signals from other signals by allowing only the signals above a certain voltage to be passed. The discriminator output is not compatible with the analyzer input requirement, and is therefore modified in a pulse inverter circuit. This circuit reverses polarity and increases the pulse amplitude.

One objective used in setting up the equipment was to minimize the duration of the electric pulse. A narrower pulse allows higher counting rates before a significant dead time correction is needed. The counting system dead time was estimated to be one μsec. This estimate is based on measurements made by Moen [20]. The highest count rate observed during the experiment was less than 10^5 counts/sec.

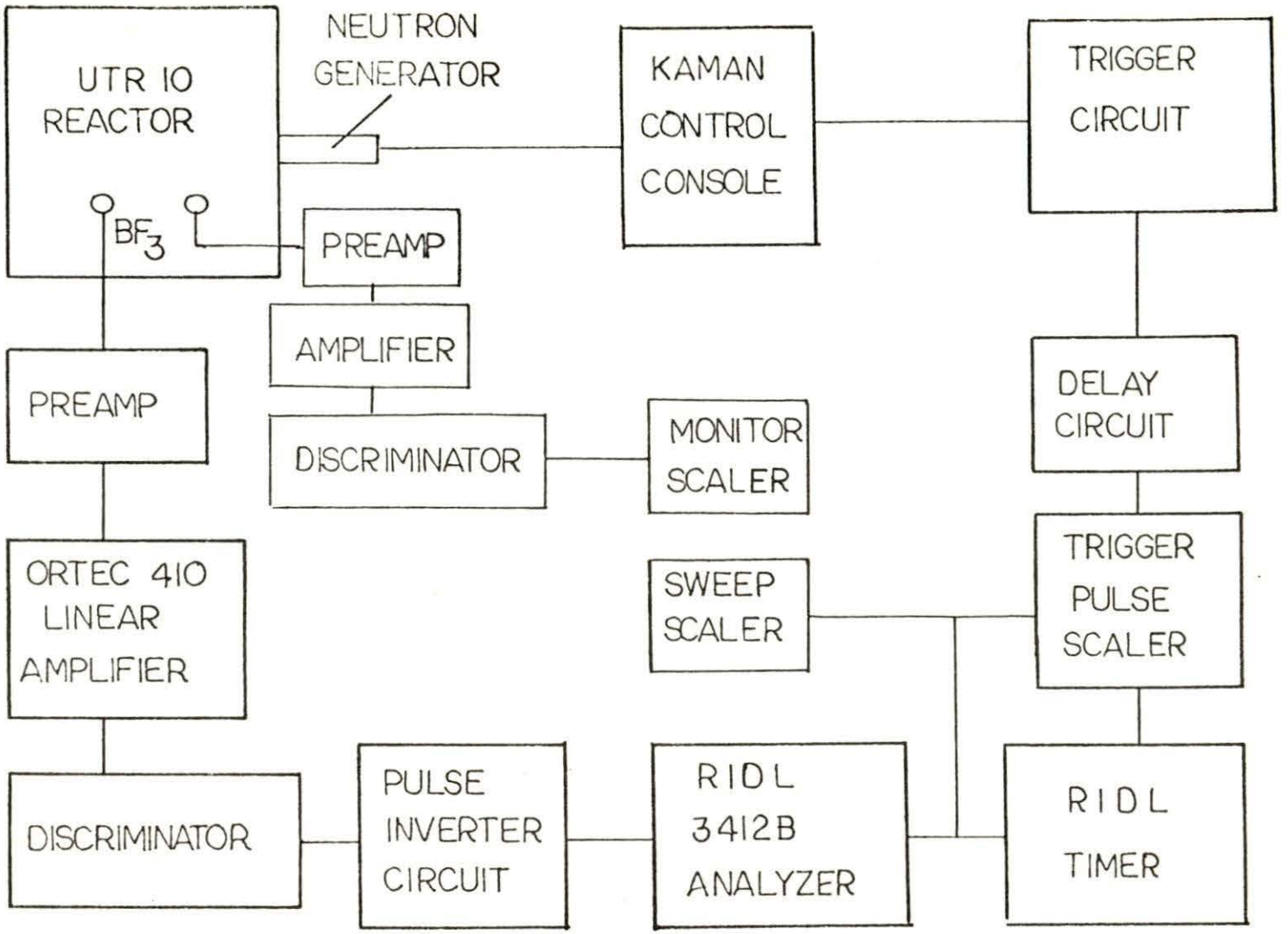

Figure 8. Block diagram of the electronic system.

Bierman et al. [4] show that for systems of this type operating at comparable count rates, the non-paralyzable formula (see Appendix C) gives a good approximation of the true count rate. For the region of the prompt fundamental decay, the dead time correction was insignificant.

The heart of the system is the RIDL model 3412B 400 channel analyzer. To properly use the analyzer, the burst of neutrons must occur at a time specified as zero. To accomplish this, a pulse from an external timer is used to trigger the neutron generator as the analyzer gate, designated as zero, opens. The external timer controls the analyzer sweep rate, and at the end of each sweep sends out a pulse. Rather than triggering the neutron generator on each sweep, the pulses are counted on a fast scaler. This scaler has been modified to produce an electronic pulse every ten sweeps. The fast scaler pulse is used to trigger the neutron generator. This means that every time the generator is triggered, the analyzer sweeps its memory ten times, then the generator is triggered again. This process is repeated until sufficient data are obtained. Use of the equipment in this manner follows the pulsed-neutron operational technique developed by Garelis [9]. This technique helps to satisfy the assumption that the pulse rate is greater than the decay constant of the shortest lived precursor. Since the pulse rate of the neutron generator is physically limited to 5 pulses/sec during continuous operation, and the decay constant of the shortest lived precursor is 4.5 sec^{-1}, multiple sweeps between neutron bursts are needed to establish a new effective pulse rate. The 100 μsec channel width

available on the analyzer timer allowed the establishment of an actual pulse rate of 2.23 pulses/sec. Based on ten sweeps of the analyzer memory for each pulse, an effective pulse rate of 22.3 pulses/sec is obtained.

Since measurements made during the initial portion of the run are made before the delayed neutrons reach equilibrium, the analyzer must remain in the store mode for a period of time after pulsing ceases. This time must be long enough to accumulate the response of the delayed neutrons.

Reactivity measurements are sensitive to the timing of the neutron burst, consequently a timing check of the pulse triggering signal and opening of channel zero was made. A variable delay circuit was used to determine that the neutron generator signal was produced approximately 5 μsec before channel zero opened. A delay circuit was used to correct for this difference. A summary of electronic settings is presented in Appendix D.

B. Methods

Prior to starting an experimental measurement, the electronic equipment was checked for operational problems. The checks consisted of inputing a square wave pulse into the amplifier and comparing the observed analyzer counts per channel with the square wave pulse rate as observed on the oscilloscope. The next procedure was to observe the neutron generator trigger pulse, the detector pulse to the analyzer, the amplifier output, the discriminator output, time base

signal, and preamp output. These signals were then compared with previous measurements.

If the electronic equipment was operating properly, the next step was to insert the BF_3 detectors into the reactor. The first pulsing attempts were performed with the neutron generator in the central stringer. The central stringer dimensions were not large enough to allow insertion of the neutron generator until the aluminum liner was removed. The removal of the 1/16 in. thick liner created a slight increase in system reactivity [7]. After the generator was filled with insulating gas, it was positioned in the central location with the aid of a graphite stringer 20 in. long. The source target was then approximately at the center plane of the core tanks. The distance from the source point to the core tanks was about 9 in.

The BF_3 detectors in the core tanks were located as shown in Figure 9, but the monitor detector was located in the thermal column.

The equipment was prepared to store data in the following manner. First the scalers, timers, and analyzers were cleared to read zero. The analyzer was then advanced to channel 399 in the store mode. The measurement was started by pushing the start button on the scaler/timer. The neutron generator fired on the first analyzer sweep because the trigger pulse scaler count advanced to one at the same time the analyzer gate zero opened. The pulsed data were then stored in the analyzer memory. The pulser stopped when the trigger pulse scaler was stopped by a preset number of counts. The analyzer memory was continued for a time long, compared to the half life of the

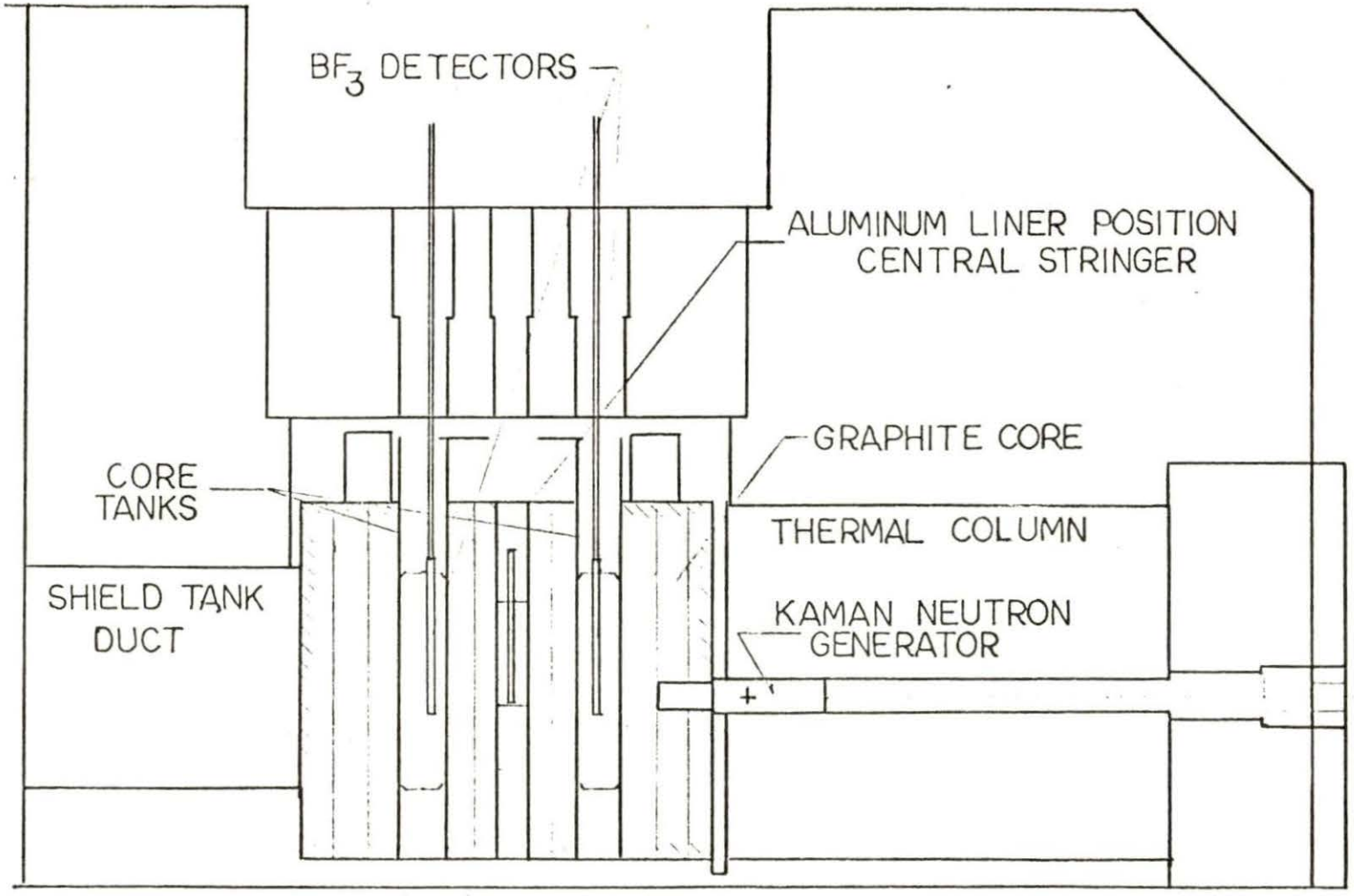

Figure 9. Cross section of the UTR-10 showing relative position of experimental equipment.

longest lived precursor. The sweeping was continued for about five minutes.

These data were then transferred to either punched tape or typed output. The next measurement made was the reactor background measurement. The best results using the GRIPE II computer program are obtained when the number of analyzer sweeps for background are the same as the pulsed data. In some cases the background measurement was only half as long, because of the long counting times required. This required an adjustment of the effective gate width (see Appendix C).

After pulsing in the central stringer was completed, the neutron generator and detectors were arranged as shown in Figure 9. The neutron source was about 24 in. from the south core tank edge. The monitor detector was positioned with the aid of two 14 in. stringers which have a 5/8 in. hole in the center to allow for the detector. The aluminum liner was left out, and only air filled the small gap left in its place. The procedures used with the pulser in this position were essentially the same as previously described.

Some problems developed with the use of this technique. In addition to component failures in the analyzer, the most serious drawback was the tendency of the detectors to pick up local radio station signals when submerged in the water. This problem was reduced by raising the discriminator level, and patching the detector's epoxy coating where pin hole leaks had developed. Even with the associated problems, the method proved to give good results.

V. RESULTS

The data obtained as counts per channel were analyzed using the GRIPE II computer program (see Appendix C). Reactivity values calculated by the program are presented in this chapter, and compared with rod drop data obtained from previous measurements and with the values suggested by the manufacturer.

The first pulsed measurements, taken with the pulser in the central stringer, were plagued by electronic noise. The extent of the noise problem in the central stringer measurements was not determined until the data were analyzed at a later time. Even with data smoothing, the constraints imposed by GRIPE II allowed only a value of zero to be calculated for α_0. Therefore, the results of the central stringer measurements are not given. Efforts to reduce the noise problem were not successful until the pulser was moved to the thermal column.

After reducing the noise problems by increasing the discriminator level and patching the cracks in the BF_3 detector's epoxy coating, the pulsing was continued, but this time from the thermal column position. The aluminum liner was left out during this series of measurements. Figures 10 through 15 show the prompt neutron response as a function of time. Negative points resulting from the subtraction of the constant reactor background and the delayed neutron background have been omitted in these plots. By plotting the various measurements on a log scale, the scatter in the data appears to increase near the end of the counting time. Figure 16, which uses a linear

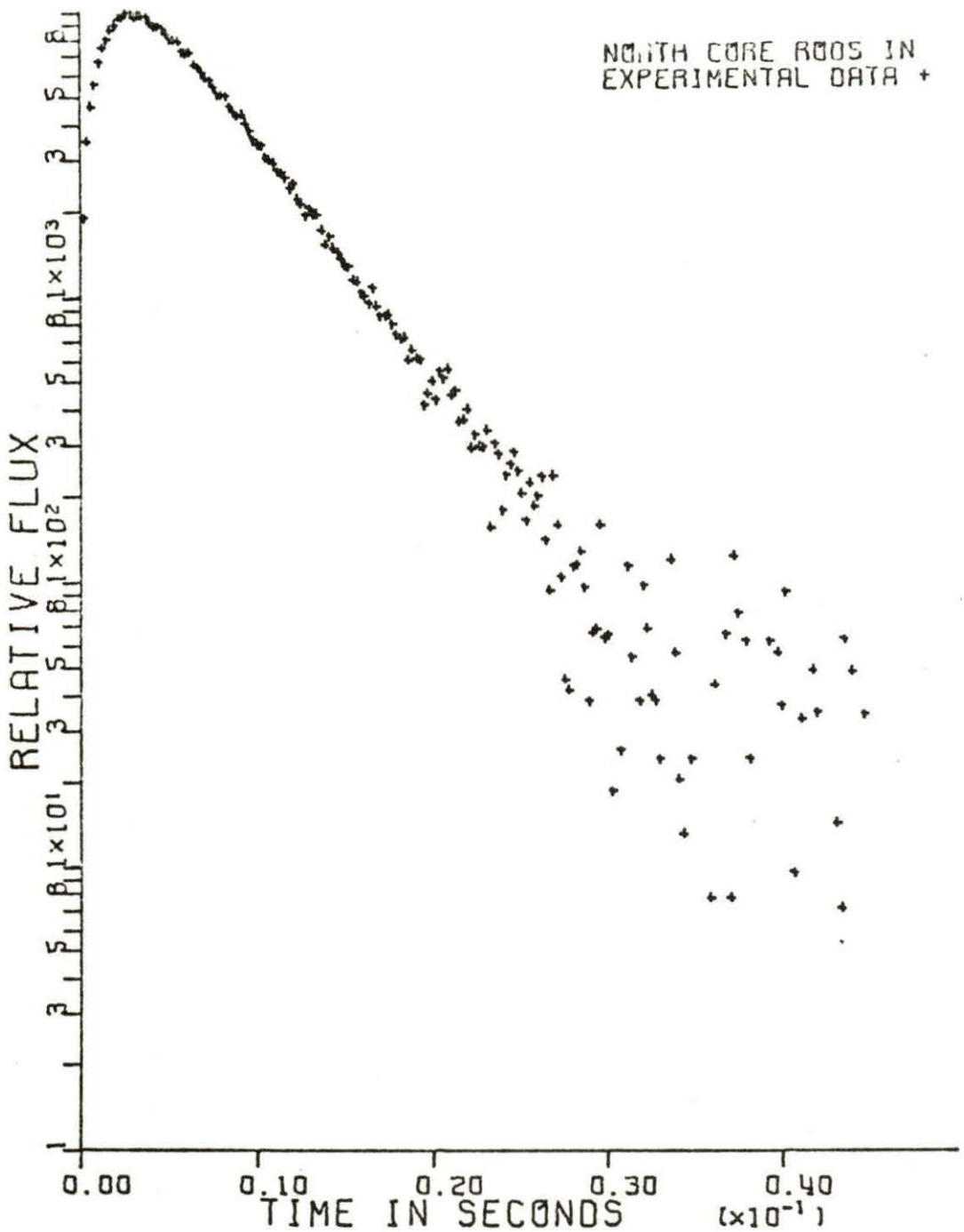

Figure 10. The prompt response of the north core with all control rods inserted.

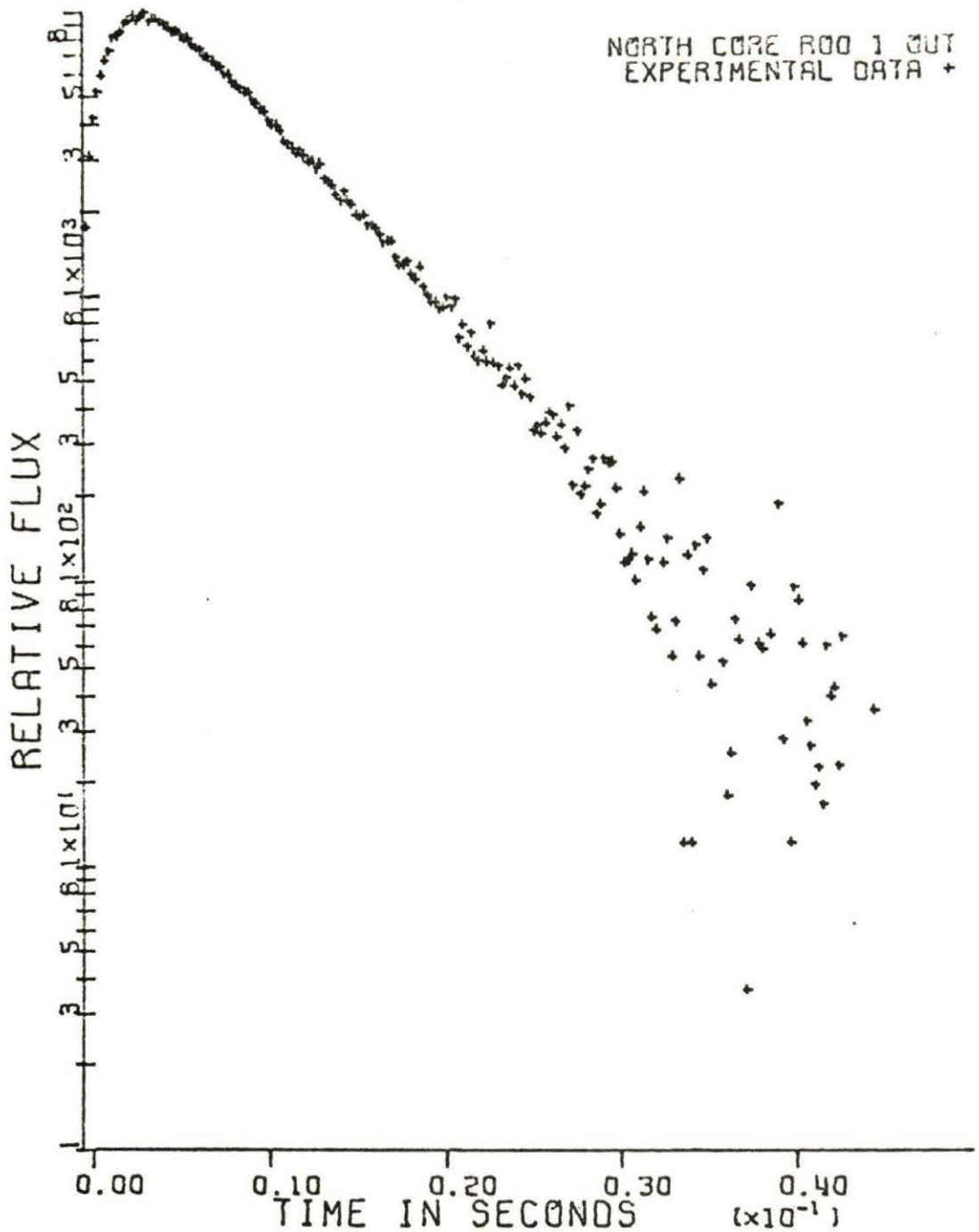

Figure 11. The prompt response of the north core with the number one safety rod withdrawn.

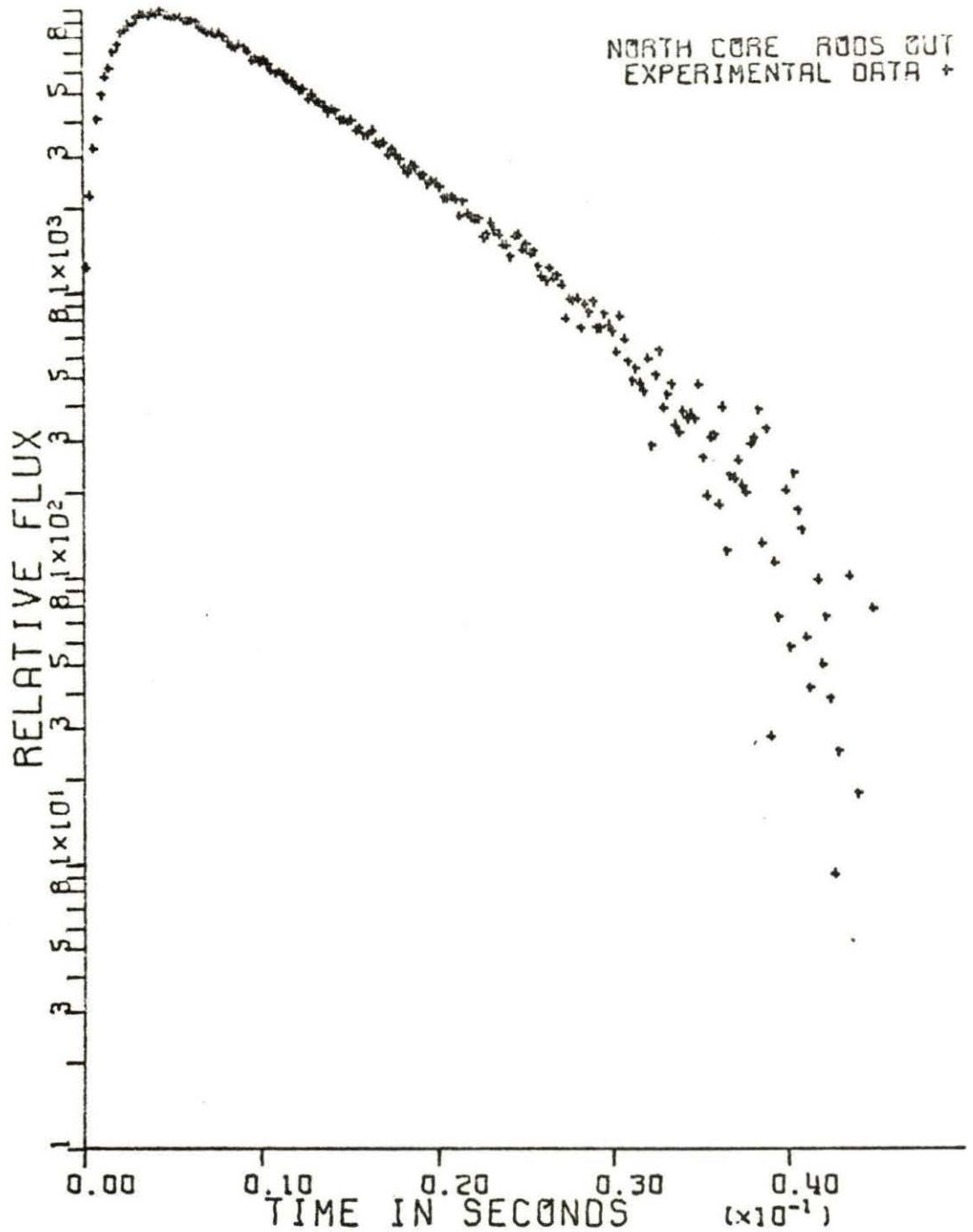

Figure 12. The prompt response of the north core with the number one and number 2 safety rod withdrawn.

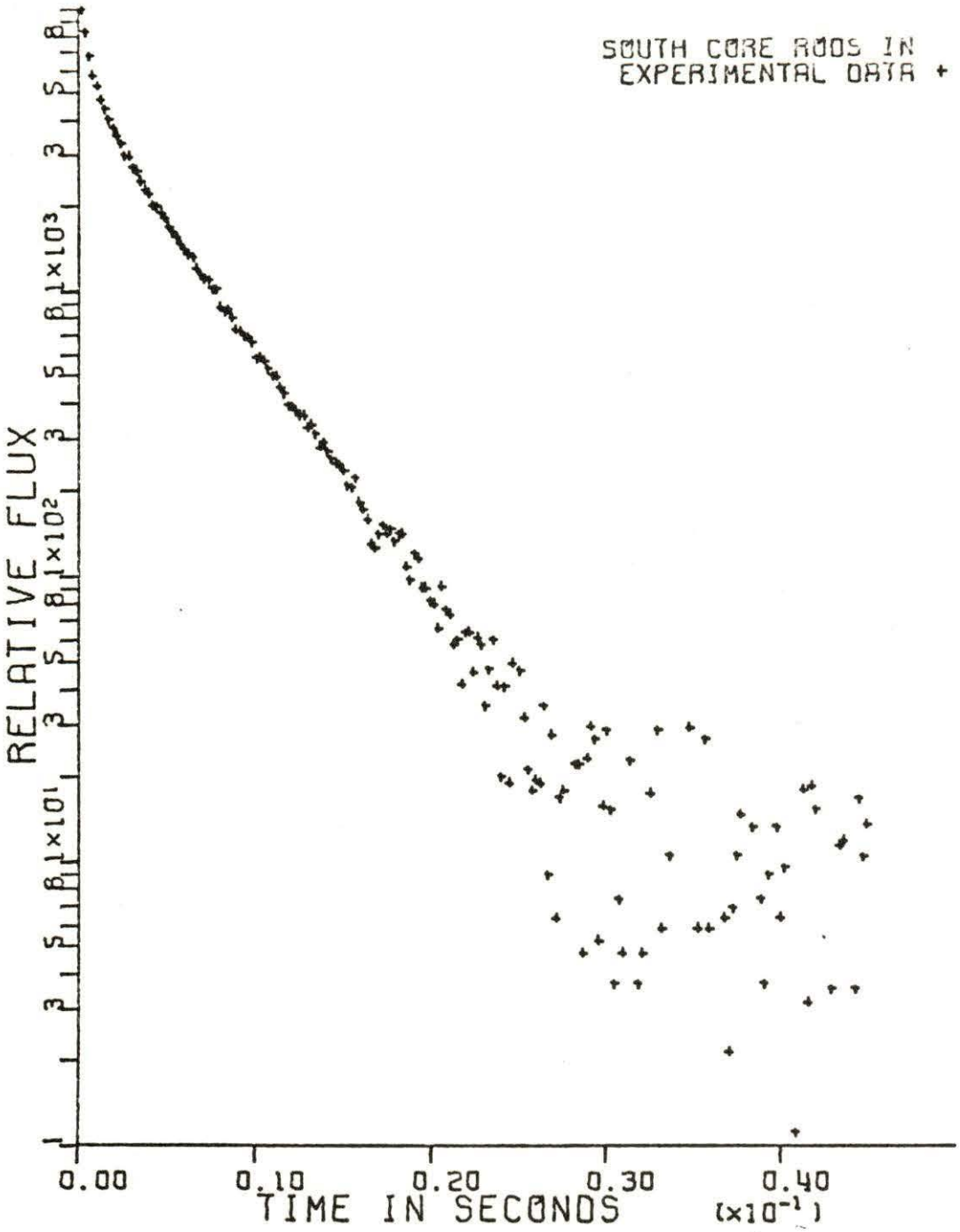

Figure 13. The prompt response of the north core with all control rods inserted.

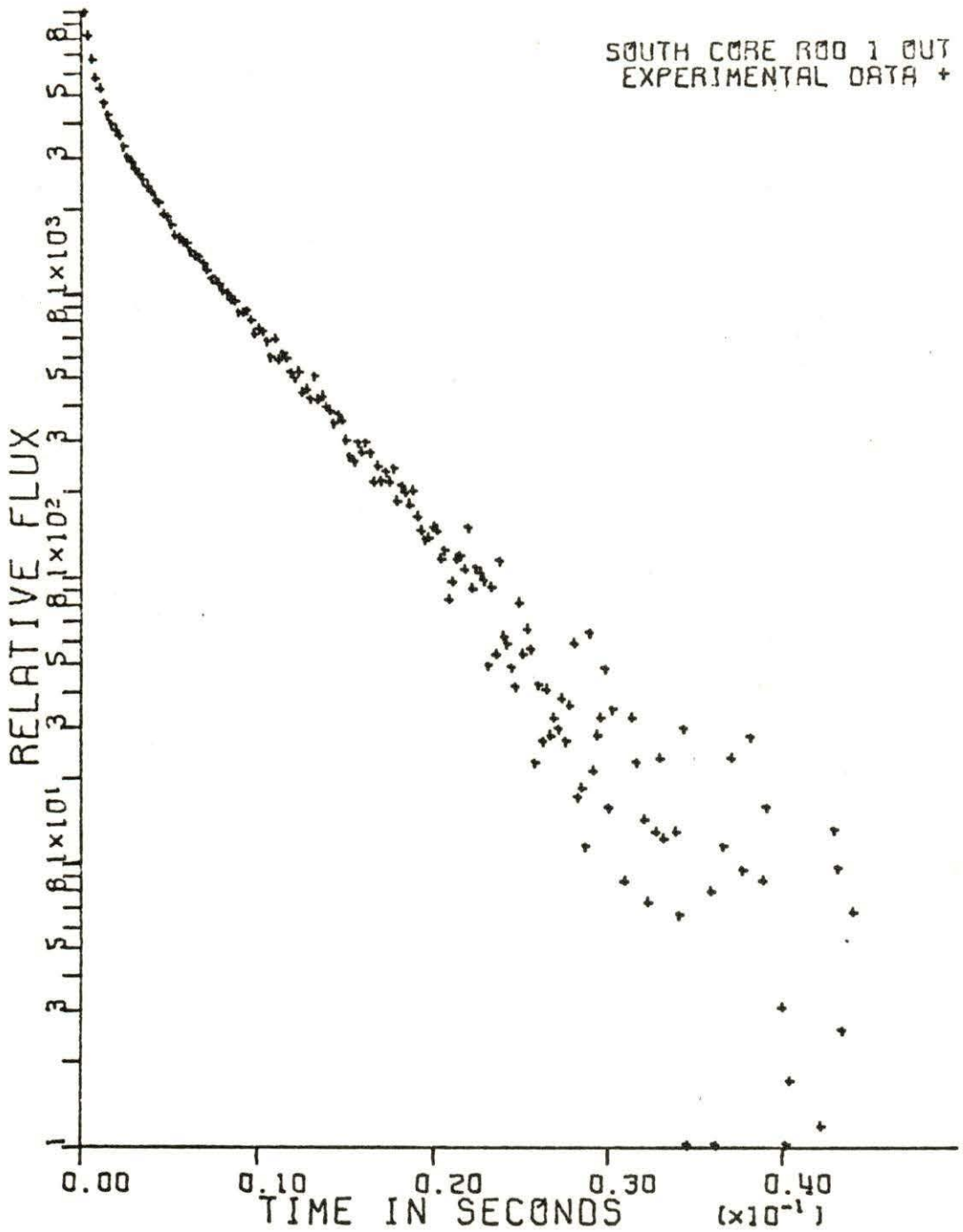

Figure 14. The prompt response of the south core with number one safety rod withdrawn.

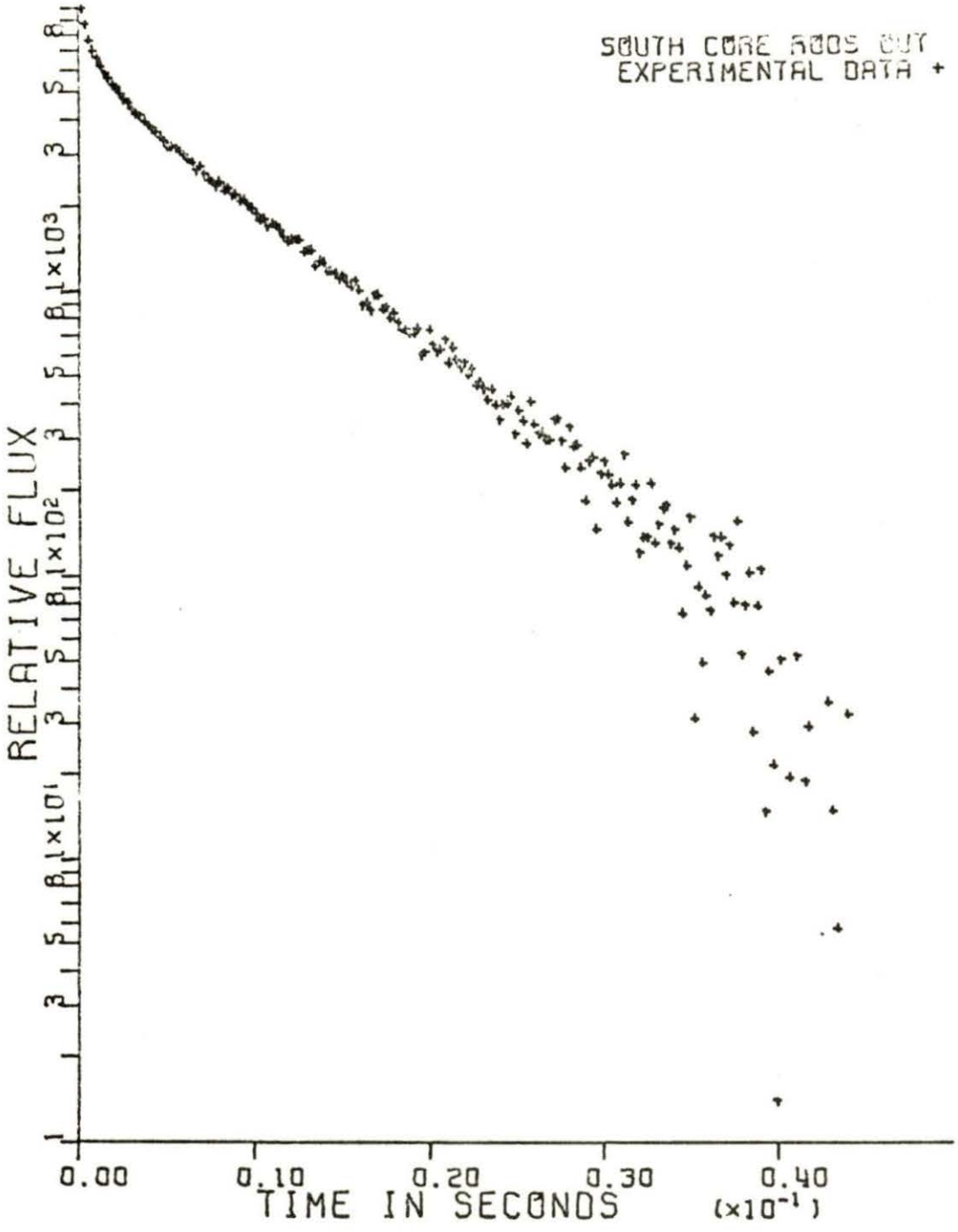

Figure 15. The prompt response of the south core with number one and number two safety rod withdrawn.

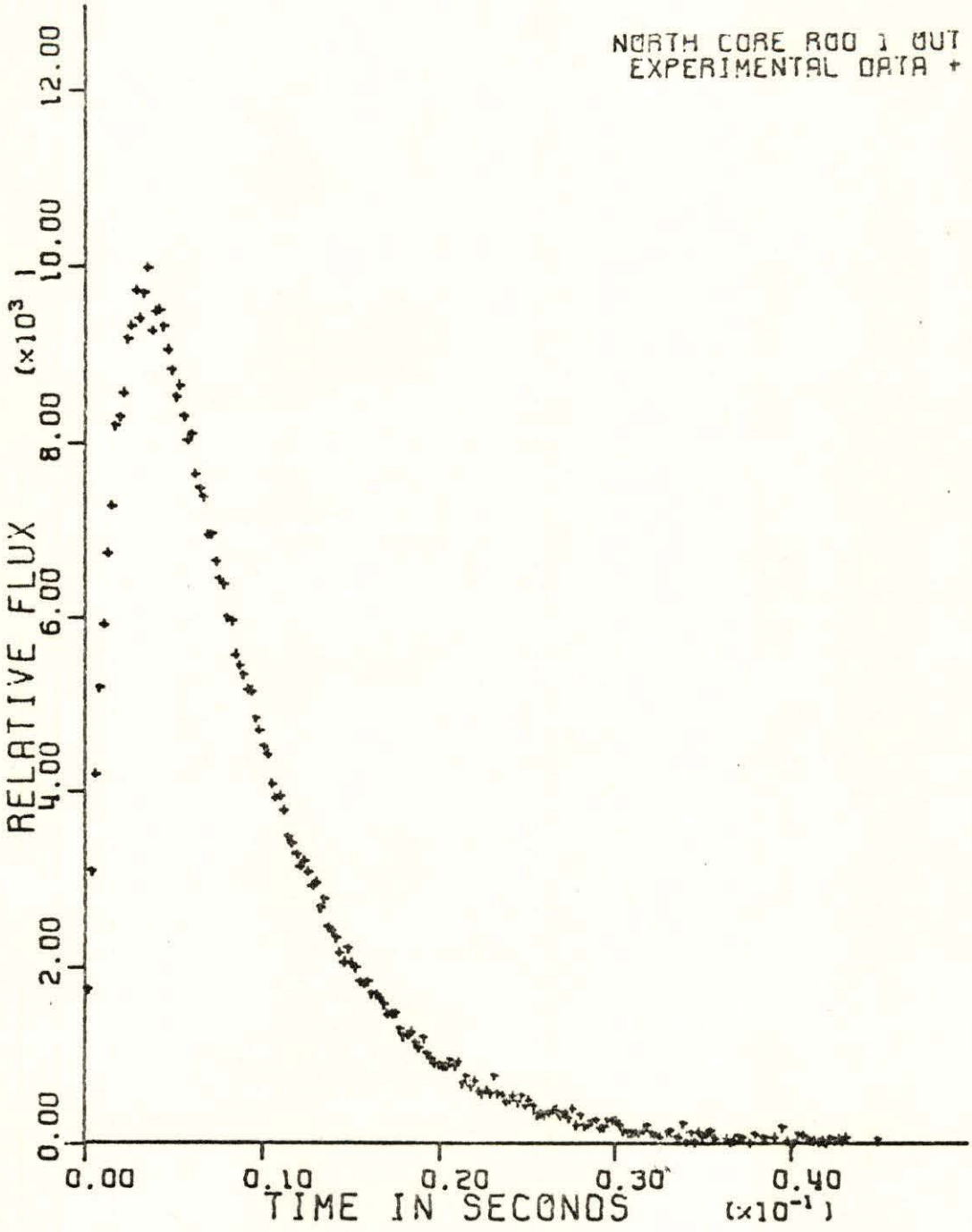

Figure 16. The data of Figure 10 plotted on a linear scale.

scale, is included to show a more representative plot of the data at the end of the prompt response.

The plots show that the decay constant decreases as the control rods are withdrawn. This was predicted by the theory developed in Chapter III. Moen [20] previously measured some decay constants for use in his frequency analysis of the UTR-10. These decay constants were on the order of 158 sec^{-1} for the north core and 163 sec^{-1} for the south core with all rods inserted. In the present study with the aluminum liner removed and the control rods in the same position, the measured α_0 was about 204 sec^{-1} in the south core, and 189 sec^{-1} in the north core. The difference in alpha did not appear as a change in reactivity since the calculated negative reactivities in Moen's study were only slightly larger. The reactivity is expected to increase when neutron absorbing material is removed. A small decrease in α_0 is also expected when absorbing material is removed. However, in this case, the large change in α_0 was accompanied by an equally large change in $k\beta/\ell$, yielding a small change in reactivity. To verify that this unexpected result was due to the removal of the aluminum liner, another pulsed-neutron measurement was made with the liner replaced. This measurement, although statistically poor, yielded an α_0 of 170 ± 11 sec^{-1} for the south core with the control rods inserted. This measurement was judged sufficient to indicate that the difference in α_0 was due to the removal of the aluminum liner. Therefore, properties other than absorption have a large effect on the decay constant and the inverse generation time. It appears that the scattering and moderating properties of aluminum, although small

compared to many other materials, are significant in the determination of parameters observed with the pulsed-neutron technique. Table II shows several common reactor materials used in the UTR-10 and some of their nuclear properties [18]. A comparison shows that aluminum does have moderating and scattering properties which are small. The center portion of the UTR-10 is the most sensitive to material changes because it is the region of the highest neutron flux. As a result the properties of the aluminum liner have a significant effect on the reactor behavior.

The removal of the aluminum liner resulted in removal of material from the reactor center which was essentially replaced with air. Since the density of air is quite low and moderating ratio, ξ, small, the resulting change could be considered as a reduction of moderating and scattering material. Therefore, it appears that α_0 is not only sensitive to reactivity changes, but also to changes in the amount of material present having moderator properties.

Table III shows the reactivities as calculated by GRIPE II for various rod positions. This shows the agreement between the different theoretical models. To compare these values with some previous measurements of rod worth, the reactivities are subtracted to obtain values of the rod worths. The standard deviations are calculated from [24, p. 61]

$$\sigma_{\text{rod worth}} = [\sigma_1^2 + \sigma_2^2]^{1/2} .$$

These values are compared with the worths measured from rod drop experiments performed as part of the reactor operational procedure in Table IV.

Table II. Nuclear properties of materials in UTR-10 [18]

Material	Density gm/cm^3	Σ_a(cm^{-1})	Σ_s(cm^{-1})	ξ^a
H_2O	1	0.0222	3.443	0.948
C	1.60	0.00027	0.08434	0.158
Al	2.699	0.01416	0.3851	0.0723

[a] ξ is a measure of the moderating power of a material and is approximately equal to $2/(A + 2/3)$ where A is the atomic mass number.

The measurements of α_0, $k\beta/\ell$, and ρ all exhibit a spatial dependence. Although only two detector positions are used to show this dependence, a comparison with the work of Ohanian and Diaz [22] shows that a dependence of this type is expected. From their study it appears that the parameters α_0, $k\beta/\ell$, and ρ all approach a constant as the distance between the detector and the pulsed source is increased. Applying this to the UTR-10 means that the best measurements are expected in the north core region. In the UTR-10, the spatial variation was most significant for α_0 and $k\beta/\ell$. The variation of these parameters tended to cancel, yielding a small variation in the reactivity as a function of position.

The techniques of Gozani and Garelis-Russell appear to agree quite well with each other and also with previously measured values, as well as those from the manufacturer. Sjöstrand's method determines reactivity values which are high in the south core and low in the north core. Since Sjöstrand's method is strongly influenced by the higher harmonics [26], it appears that the larger reactivities

Table III.[a] Prompt decay constant, α, inverse generation time, β/Λ, and reactivity ρ[b] as measured in the north and south core with the pulser in the thermal column.

Control rod position	$\alpha_0(sec^{-1})$	South core $\beta/\Lambda(sec^{-1})$ G - R	$\rho_{GOZ}(\$)$	$\rho_{G-R}(\$)$	$\rho_{Sj}(\$)$
Rods in	204.26 ± 0.97	51.36 ± 0.44	2.90 ± 0.03	2.98 ± 0.04	3.43 ± 0.03
Safety #1 out	177.83 ± 6.80	51.05 ± 0.35	2.08 ± 0.08	2.12 ± 0.08	2.45 ± 0.08
Safety #1 and #2 out	103.94 ± 1.53	53.20 ± 0.33	0.942 ± 0.009	0.953 ± 0.019	1.05 ± 0.01

Control rod position	$\alpha_0(sec^{-1})$	North core $\beta/\Lambda(sec^{-1})$ G - R	$\rho_{GOZ}(\$)$	$\rho_{G-R}(\$)$	$\rho_{Sj}(\$)$
Rods in	189.22 ± 1.04	48.42 ± 0.37	3.08 ± 0.04	2.90 ± 0.04	2.21 ± 0.04
Safety #1 out	155.61 ± 0.07	50.45 ± 0.23	2.19 ± 0.02	2.08 ± 0.02	1.60 ± 0.02
Safety #1 and #2 out	104.10 ± 0.54	53.68 ± 0.17	0.959 ± 0.004	0.939 ± 0.006	0.756 ± 0.004

[a] Standard deviations given are the result of counting statistics as calculated by GRIPE II.

[b] The kinetic distortion factor is assumed to be one.

Table IV. Comparison of rod worths calculated by different methods.

Method	Safety #1 ($)	Safety #2 ($)
Sjöstrand from south core	0.978 ± 0.085	1.40 ± 0.08
Sjöstrand from north core	0.604 ± 0.038	0.846 ± 0.035
Gozani from south core	0.810 ± 0.085	1.14 ± 0.08
Gozani from north core	0.896 ± 0.038	1.22 ± 0.04
Garelis-Russell from south core	0.860 ± 0.089	1.16 ± 0.04
Garelis-Russell from north core	0.823 ± 0.036	1.04 ± 0.02
Rod drop experiment	~ 0.824	~ 1.015
Manufacturer[b] listed value	~ 0.97	~ 0.97

[a]Performed as part of the reactor operational procedure, August 1970.

[b]Based on $\beta = 0.0064$ [1, 18, 21].

measured by this method in the south core indicate that positive higher harmonics exist at this location. The smaller reactivities measured in the north core indicate that negative harmonics exist in this region following the burst of neutrons. The small spatial dependence of reactivity in the high absorption regions, as determined by both the methods of Gozani and Garelis-Russell, is apparently the result of both higher harmonics and the difference in the delayed and prompt modes as discussed in Chapter II. Both methods appear to eliminate

the problem of higher harmonics [11, 12]. Danofsky [6] made test runs using the detector located in the central stringer. The reactivity, as calculated by the methods of Gozani and Garelis-Russell, measured in this region was much higher than corresponding fuel region measurements. This indicates that in the low absorption region, the kinetic distortion factor is greater, as predicted by Preskitt et al. [23]. A calculation of the kinetic distortion factor would be needed to correct the measured reactivities for a determination of the reactivity.

VI. SUMMARY AND CONCLUSIONS

The results of this thesis verify that the pulsed-neutron technique can be used to measure reactivities in a subcritical reactor. The methods of Gozani and Garelis-Russell appear to behave in a similar manner, but Sjöstrand's dependence on the higher harmonics shows the greatest spatial dependence. The kinetic distortion factor influences the calculations of both the Gozani and Garelis-Russell techniques. It is felt that by placing the detectors in the high absorption region the kinetic distortion factor was reduced to the minimum.

The value of the decay constant, α_0, depends not only on reactivity changes, but on other material properties as well. More data correlating changes in materials with differences in the decay constant are needed before definite conclusions can be made.

Because of the results obtained in this study, as well as the results of other investigators, it is felt that the pulsed-neutron technique could be used as a non-destructive method to measure the properties of reactor fuel elements, possibly fuel enrichment. Experiments could be performed to determine the relative magnitudes of α_0, $k\beta/\ell$, and ρ for an assembly of elements in a test facility. Care in building an assembly with a keff $\cong$ 0.9 must be exercised because of criticality considerations. Keepin [15] points out that in reflected systems the measurements are limited by the characteristic decay of the moderator to about \$15 subcritical. However, Fieno et al. [8] have measured reactivities up to \$50 in a bare solution reactor. Preskitt et al. [23] point out that reactivity does not have to be the focal point of reactor experiments.

This information leads to the conclusion that an experimental method could possibly be developed to correlate the observable quantities of the pulsed-neutron experiment to fuel element enrichment.

VII. SUGGESTIONS FOR FUTURE WORK

Several items that would be of interest for future investigators have resulted from this work. The following list indicates some of the possible areas that could be studied.

1. A method is needed for the determination of the kinetic distortion factor applied to the UTR-10.

2. Experiments could be performed to determine the variations of the decay constant measurement as a function of source position, and material changes in the central stringer. This could be used to study the variation in the decay constant due to changes in absorbtion and moderation properties.

3. Procedures and testing methods are needed to develop the role of the pulsed-neutron technique for the determination of fuel element enrichment. This concept is discussed in Chapter VI.

4. Additional pulsed-neutron measurements could be made with detectors in different locations. These measurements could be compared with previous measurements to determine the spatial flux shape as a function of time following a burst of neutrons.

VIII. LITERATURE CITED

1. AMERICAN STANDARD COMPANY, Advanced Technology Laboratories Division, Operating Manual for the UTR-10 Reactor, Mountain View, Calif., (1959).

2. M. BECKER and K. S. QUISENBERRY, "Spatial Dependence of Pulsed Neutron Reactivity Measurements," AEC Symposium Series No. 7, (1966).

3. J. M. BETANCOURT, "Analysis of Coupled Core Reactors Using the Natural Mode Approximation," PhD Dissertation, Iowa State University (1968).

4. S. R. BIERMAN, K. L. GARLID, and J. R. CLARK, Nuclear Applications, 2 515 (1966).

5. J. R. BROWN, "Measurements of Subcritical Reactivity Using a Pulsed Neutron Source," AT (04-3)-167, General Atomic Division of General Dynamics (1964).

6. R. A. DANOFSKY, "Kinetics of Coupled-Core Reactors," Engineering Research Institute, Iowa State University (1970).

7. R. A. DANOFSKY, Personal Communication (June 1971).

8. D. FIENO, T. A. FOX, R. A. MUELLER, and C. H. FORD, "Determination of Reactivities Using Pulsed Neutron Techniques for Highly Subcritical Solution Reactors," NASA TMX 52369, Lewis Research Center, Cleveland, Ohio (1967).

9. EDWARD GARELIS, Nucl. Sci. Eng., 18 242 (1964).

10. E. GARELIS and P. MEYER, "Development of Pulsed Neutron Application to Power Reactor Start Up Procedures," GEAP-4606, General Electric Atomic Power Equipment Department, San Jose, Calif., (1964).

11. E. GARELIS and JOHN RUSSELL, JR., Nucl. Sci. Eng., 16 263 (1963).

12. TSAHI GOZANI, "The Theory of the Modified Pulsed Source Technique," EIR-Bericht Nr. 79, Eidg. Institut für Reaktorforschung Würenlingen Schweiz (1965).

13. KAMAN SCIENCES CORP., Kaman Nuclear Division, Instruction Manual for Model A-800/801 Neutron Generator, Colorado Springs, Colorado, Author (ca. 1969).

14. N. C. KAUFMAN, "A Computer Program for the Analysis of the Data from a Pulsed Neutron Experiment," IN-1085, Idaho Nuclear Corp. (1967).

15. G. R. KEEPIN, Physics of Nuclear Kinetics, pp. 221-281, Addison-Wesley Publishing Co., Reading, Mass. (1966).

16. O. C. KOLAR and F. A. KLOVERSTROM, Nucl. Sci. Eng., 10 45 (1961).

17. M. B. KRATZER, Nuclear News 14 40 (1971).

18. JOHN LAMARSH, Introduction to Nuclear Reactor Theory, pp. 417-520, Addison-Wesley Publishing Co., Reading, Mass. (1966).

19. C. F. MASTERS and K. B. CADY, Nucl. Sci. Eng., 29 272 (1967).

20. D. A. MOEN, Personal Communication (June 1971).

21. D. A. MOEN, "Reactor Frequency Response Based on the Pulsed Neutron Technique," Unpublished PhD Dissertation, Iowa State University, (1971).

22. M. J. OHANIAN and N. J. DIAZ, "Final Report on Research on Neutron Pulse Propagation in Multiplying Media for Idaho Nuclear Corp.," Contract Nos. 0-281 and 0-635, University of Florida (1969).

23. C. A. PRESKITT et al., Nucl. Sci. Eng., 29 283 (1967).

24. WILLIAM PRICE, Nuclear Radiation Detection, 2nd ed., McGraw Hill, New York, New York, (1964).

25. B. E. SIMMONS and J. S. KING, Nucl. Sci. Eng., 3 595 (1958).

26. N. G. SJÖSTRAND, Arkiv Fysik, 11 233 (1956).

27. F. A. VALENTI, A Manual of Experiments in Reactor Physics, pp. 94-124, Macmillan, New York (1963).

IX. ACKNOWLEDGMENTS

The author wishes to express his gratitude to his major professor, Dr. Richard Danofsky, whose guidance and encouragement made this work possible. In addition, the author expresses appreciation to the National Science Foundation for providing Dr. Danofsky with the funds, part of which were used as a graduate assistantship, to study the kinetics of coupled core reactors. Thanks are also due to Dr. Glenn Murphy, Head of the Nuclear Engineering Department, for making available the departmental facilities used in this work.

In conclusion, the author wishes to acknowledge his wife, Beth, for her efforts to make continued study possible.

X. APPENDIX A

To understand the $k\beta/\ell$ technique, it is important to understand the assumptions leading to the development. This Appendix follows the development of Garelis and Russell, and the symbols used follow the original reference [11].

Consider the time dependent neutron density $N(x, x', t)$, at some point x due to a source at x', at time t. Then the time-dependent neutron diffusion and precursor equations are given by

$$-\left(\frac{M^2}{\ell_0}\right)\frac{\partial^2 N}{\partial x^2} + [1 - k_0(1 - \beta)](N/\ell_0) + \frac{\partial N}{\partial t} - \sum_{i=1}^{M} \lambda_i C_i = s(x, x', t) \tag{A-1}$$

and

$$\frac{\partial C_i}{\partial t} = -\lambda_i C_i + k_0 \beta_i (N/\ell_0) \qquad i = 1, 2, \ldots, m. \tag{A-2}$$

where M^2 is the migration area[a], $k_0(\ell_0)$ the infinite medium multiplication constant (lifetime), C_i the i^{th} delayed precursor concentration, $\beta = \Sigma\beta_i$ the total delayed fraction, and $s(x, x', t)$ represents the source. For a pulsed source, pulsed at the rate R pulses per second,

$$S(x, x'; t) = \delta(x - x') \sum_{n=0}^{\infty} \delta(t - \tfrac{n}{R}). \tag{A-3}$$

This system of equations is solved for N with the use of the Laplace transform, application of boundary conditions for a bare slab reactor, and applying the orthogonality property to expand the source as a series of sin functions. The solution is

---

[a] M^2 is used instead of L^2 to account for the fast neutron losses due to diffusion.

$$\bar{N} = \frac{2}{a} \sum_{n=1}^{\infty} \left\{ \frac{\sum_{i=0}^{\infty} e^{-s_i/R}}{[1 - k_n/\ell_n] + S + (\frac{k_n}{\ell_n}) \sum_{i=1}^{m} \frac{s\beta_i}{s + \lambda_i}} \right\} \cdot \sin B_n x \sin B_n x', \tag{A-4}$$

where a is the extrapolated slab thickness, $k_n = k_0/1 + M^2B_n^2$, $\ell n = \ell_0/1 + M^2B_n^2$, s is the Laplace transform variable, and B_n the familiar buckling term.

In order to simplify the notation let $\psi_n(x) = \sqrt{2/a} \sin B_n x$ and consider only one mode N_n, thereby eliminating the first summation.

$$\bar{N}_n = \Pi_{j=1}^{m} \frac{(s + \lambda_i) \sum_{i=0}^{\infty} e^{-s_i/R} \psi_n(x) \psi_n(x')}{\Pi_{j=1}^{m+1} (s - a_{jn})} \tag{A-5}$$

where a_{jn} are the roots of the denominator of Eq. (A-4) which is the usual inhour equation. Applying the inversion theorem to Eq. (A-5) by expanding the series as a sum of partial fractions yields

$$N(x, x'; t) = \psi_n(x)\psi_n(x') \sum_{r=0}^{\infty} \sum_{s=1}^{m+1} \frac{\Pi_{j=1}^{m} (a_{sn} + \lambda_j)}{\Pi_{j=1 \; j\neq s}^{m+1} (a_{sn} - a_{jn})} \cdot e^{(t - r/R/a_{sn}} H(t - r/R). \tag{A-6}$$

Here H(t - r/R) is a function which equals 1 for $t > 0$ and 0 for $t < 0$, and r is the number of pulses.

Let the assembly be pulsed for K + 1 pulses, then $t = K/R + \tau$ $0 < \tau < 1/R$, then summing the resulting series, Eq. (A-6) becomes

$$N_n = \psi_n(x)\psi_n(x') \sum_{s=1}^{m+1} \frac{e^{a_{sn}\tau} \Pi_{j=1}^{m} (a_{sn} + \lambda_j)}{\Pi_{j=1 \; j\neq s}^{m+1} (a_{sn} - a_{jn})} \cdot \left(\frac{e^{\frac{ka_{sn}}{R}} - e^{\frac{-a_{sn}}{R}}}{1 - e^{\frac{-a_{sn}}{R}}} \right). \tag{A-7}$$

This represents the solution to the neutron diffusion equations, which can be simplified with the following assumptions.

Since the assembly is subcritical, all the roots of the inhour equation are negative, hence K can be chosen so that $\exp(Ka_{sn}/R)$ can be neglected in comparison to $\exp(-a_{sn}/R)$ in Eq. (A-7). This defines the quasi-equilibrium condition, i.e.

$$\exp[a_{sn}(K + 1)/R] \ll 1. \tag{A-8}$$

When $K \gg 1$, $(K + 1)/R$ is approximately equal to the elapsed time. Therefore, Eq. (A-8) is also represented by $\exp(a_{sn}T) \ll 1$ where T represents the elapsed time. With the exception of the prompt root, the roots of the inhour equation all approach the decay constant of the precursors, i.e., $|a_{sn}| \to \lambda_s$. Therefore, for times, T, long compared to the 55 sec half life of the longest lived precursor, the quasi equilibrium condition will be established. This holds true for typical water systems more than \$1 subcritical.

Equation (A-7) can be written as

$$N_n = \left\{ \frac{-e^{a_{1n}\tau} \prod_{j=1}^{m} (a_{1n} + \lambda_i)}{\prod_{j=2}^{m+1} (a_{1n} - a_{jn})} \cdot \left(\frac{e^{\frac{-a_{1n}}{R}}}{1 - e^{\frac{-a_{1n}}{R}}} \right) \right. \tag{A-9}$$

$$\left. - \sum_{s=2}^{m+1} \frac{e^{a_{sn}\tau} \prod_{j=1}^{m} (a_{sn} + \lambda_i)}{\prod_{j=1 \; j\neq s}^{m+1} (a_{sn} - a_{jn})} \cdot \left(\frac{e^{\frac{-a_{sn}}{R}}}{1 - e^{\frac{-a_{sn}}{R}}} \right) \right\} \psi_n(x) \psi_n(x')$$

where s = 1 is the prompt contribution, the first term in Eq. (A-9). Assuming that $|a_{1n}|/R \gg 1$, then the exponential in the brackets can be replaced by - 1 since all $a_{sn} < 0$ for a subcritical assembly.

Further assume that the prompt root is dominant, i.e.,

$$|a_{1n}| \gg |a_{jn}|, \qquad j = 2, 3, \ldots, m+1,$$

and the quotient of product terms can be replaced by + 1. This approximation is worst for the shortest lived precursor, $\lambda = 4.5\ \text{sec}^{-1}$, and since its yield is low, the inhour root corresponding to the precursor is close to - 4.5; hence this contribution in the quotient of Eq. (A-9) tends to cancel. With these assumptions the prompt contribution is given by

$$N_p = e^{a_{1n}\tau}\psi_n(x)\psi_n(x'). \tag{A-10}$$

Next consider the delayed contribution, which is the second term in Eq. (A-9), time averaged over one cycle

$$\langle N_{dn} \rangle = R \int_0^{1/R} N_{dn}\, d\tau \quad . \tag{A-11}$$

Carrying out the integration yields (apart from the sign)

$$\langle N_{dn} \rangle = R \sum_{s=2}^{m+1} \frac{\prod_{j=1}^{m} (a_{sn} + \lambda_j)\psi_n(x)\psi_n(x')}{a_{sn} \prod_{\substack{j=1 \\ j\neq s}}^{m+1} (a_{sn} - a_{jn})} \quad . \tag{A-12}$$

Under the conditions of a pulsed experiment, the pulse rate is such that $|a_{sn}|\ 1/R \ll 1\ s \neq 1$ so that

$$e^{s_{an}\tau}\left(\frac{e^{\frac{-a_{ns}}{R}}}{1 - e^{\frac{-a_{sn}}{R}}}\right) \simeq \frac{R}{a_{sn}}\left[1 + (\tau R - \frac{1}{2})\frac{a_{sn}}{R} + \left[\frac{1}{12} - \frac{\tau R}{2} + \frac{(\tau R)^2}{2}\right]\right.$$
$$\left.(\frac{a_{sn}}{R})^2\right] \tag{A-13}$$

where it is assumed that $\tau < 1/R$. Then for pulse rates of $R \geq 10$ the approximation is valid as discussed in Ref. [9].

Equation (A-9) can then be simplified to become

$$N_n = e^{a_{1n}\tau} - \sum_{s=2}^{m+1} \left[\frac{R}{a_{sn}} + (\tau R - \frac{1}{2})\right] \cdot \frac{\prod_{j=1}^{m}(a_{sn} + \lambda_i)}{\prod_{j=1, j\neq s}^{n+1}(a_{sn} - a_{jn})} \tag{A-14}$$

where the factor $\psi_n(x)\psi_n(x')$ is omitted for convenience. By assuming that

$$\frac{\prod_{j=1}^{m}(a_{1n} + \lambda_i)}{\prod_{j=2}^{m+1}(a_{1n} - a_{jn})} \simeq 1$$

and performing some algebraic expansions, Garelis and Russell [11] show that Eq. (A-14) becomes

$$N_n = e^{a_{1n}\tau} + R\ell_n/(1 - k_n) + R/a_{1n}, \tag{A-15}$$

by defining $\$ = (1 - k_n)/k_n\beta$, Eq. (A-15) can be written as

$$N_n = e^{-\alpha_n t} + R/\alpha_n\$_n$$

where $a_{1n} = -\alpha_n$. Then the final expression for the neutron density, summing over all the modes, is

$$N = \sum_{n=1}^{\infty}\left[e^{-\alpha_n\tau} + \frac{R}{(\alpha_n\$_n)}\right]\psi_n(x)\psi_n(x'), \tag{A-16}$$

or

$$N = N_p + N_d \tag{A-17}$$

where

$$N_p = \sum_{n=1}^{\infty} e^{-\alpha_n\tau}\psi_n(x)\psi_n(x') \tag{A-18}$$

and

$$N_d = R \sum_{n=1}^{\infty} \psi_n(x)\psi_n(x')/(\alpha_n \$_n) \tag{A-19}$$

Now consider the following integral

$$I_1 = \int_0^{1/R} N_p d\tau \tag{A-20}$$

Since $\alpha_n/R \gg 1$, Eq. (A-20) can be written as

$$I_1 = \int_0^{\infty} N_p d\tau = \sum_{n=1}^{\infty} \psi_n(x)\psi_n(x')/\alpha_n \tag{A-21}$$

Similarly, consider

$$I_2 = \int_0^{\infty} N_p[\exp(k_1\beta/\ell_1)\tau]d\tau, \tag{A-22}$$

where 1/R is replaced with ∞ since the contribution to the integral after 1/R is approximately zero. Since (k_1/ℓ_1) is independent of spatial modes, Eq. (A-22) can be written as

$$I_2 = \sum_{n=1}^{\infty} \psi_n(x)\psi_n(x') \int_0^{\infty} \exp[-\tau(1 - k_n)/\ell_n]d\tau \tag{A-23}$$

$$= \sum_{n=1}^{\infty} \psi_n(x)\psi_n(x')\ell_n/(1 - k_n).$$

Subtracting I_1 from I_2 yields

$$I_1 - I_2 = \sum_{n=1}^{\infty} \psi_n(x)\psi_n(x') \left[\frac{\ell_n}{1 - R_n} - \frac{1}{\alpha_n}\right]. \tag{A-24}$$

Noting that $(\ell_n/1 - R_n) - (1/\alpha_n) = 1/\alpha_n \$_n$ and comparing with Eq. (A-19) yields

$$I_1 - I_2 = \frac{1}{R} N_d \tag{A-25}$$

which is the desired result, often written as

$$\int_0^\infty N_p \exp\left[\frac{k\beta}{\ell} t\right] dt - \int_0^\infty N_p dt = \frac{N_d}{R} \qquad \text{(A-26)}$$

The solution of this equation determines $k\beta/\ell$ from experimental data and reactivity can be found from

$$\$ = [\alpha_1 - (k_1\beta/\ell_1)]/(k_1\beta/\ell_1). \qquad \text{(A-27)}$$

where the subscript 1 represents the fundamental mode.

XI. APPENDIX B

Following the method developed by Gozani [12] this appendix shows how the extrapolated area ratio method is developed. The symbols used here are the same as those used in the original paper. Gozani starts with the point reactor equations

$$\frac{dn}{dt} = \frac{\rho - 1}{\Lambda^*} n + \sum_{i=1}^{\ell} \lambda_i C_i + Q(t) \qquad \text{(B-1)}$$

and

$$\frac{dC_i}{dt} = \frac{b_i}{\Lambda^*} n - \lambda_i C_i \qquad i = 1, 2, \ldots \ell. \qquad \text{(B-2)}$$

The terms in these equations are $\Lambda^* = \Lambda/\beta$, $b_i = \beta_i/\beta$, ρ = reactivity in dollars (ρ/β), $\beta = \sum_{i=1}^{\ell} \beta_i$, $b = \sum_{i=1}^{\ell} b_i = 1$, and $Q(t)$ is the external source. Next the equations are Laplace transformed to solve for N. Equations (B-1) and (B-2) become respectively

$$sN(s) = \frac{\rho - 1}{\Lambda^*} N(s) + \sum_{i=1}^{\ell} \lambda_i C_i(s) + Q(s), \qquad \text{(B-3)}$$

and

$$sC_i(s) = \frac{b_i}{\Lambda^*} N(s) - \lambda_i C_i(s). \qquad \text{(B-4)}$$

Solving for $C_i(s)$ in Eq. (B-4) and substituting back into Eq. (B-3) yields

$$N(s)\left[s - \frac{\rho - 1}{\Lambda^*} - \sum_{i=1}^{\ell} \frac{\lambda_i b_i}{\Lambda^*(s + \lambda_i)}\right] = Q(s). \qquad \text{(B-5)}$$

Note that in Eq. (B-5) the term

$$\left[s - \frac{\rho - 1}{\Lambda^*} - \sum_{i=1}^{\ell} \frac{\lambda_i b_i}{\Lambda^*(s + \lambda_i)}\right]$$

may be written as

$$\left[s - \frac{\rho}{\Lambda^*} + \frac{1}{\Lambda^*} \sum_{i=1}^{\ell} b_i - \frac{1}{\Lambda^*} \sum_{i=1}^{\ell} \frac{\lambda_i b_i}{s + \lambda_i} \right]$$

since

$$\sum_{i=1}^{\ell} b_i = 1.$$

Combining terms yields

$$\left[s - \frac{\rho}{\Lambda^*} + \frac{1}{\Lambda^*} \sum_{i=1}^{\ell} \frac{s b_i}{s + \lambda_i} \right].$$

Therefore Eq. (B-5) becomes

$$\frac{N(s)}{\Lambda^*} \left\{ s \left[\Lambda^* + \sum_{i=1}^{\ell} \frac{b_i}{s + \lambda_i} \right] - \rho \right\} = Q(s). \qquad \text{(B-6)}$$

Solving Eq. (B-6) for N(s) yields

$$N(s) = \Lambda^* Q(s) \left\{ s \left[\Lambda^* + \sum_{i=1}^{\ell} \frac{b_i}{s + \lambda_i} \right] - \rho \right\}^{-1}. \qquad \text{(B-7)}$$

Let

$$G(s) = \left\{ s \left[\Lambda^* + \sum_{i=1}^{\ell} \frac{b_i}{s + \lambda_i} \right] - \rho \right\}^{-1},$$

and note that

$$G(t) = \sum_{j=0}^{\ell} A_j e^{\gamma_j t} \qquad \text{(B-8a)}$$

where γ_j are the roots of the inhour equation

$$\rho = s \left\{ \Lambda^* + \sum_{i=1}^{\ell} \frac{b_i}{s + \lambda_i} \right\}, \qquad \text{(B-8b)}$$

and

$$A_j^{-1} = \Lambda^* + \sum_{i=1}^{\ell} \frac{b_i \lambda_i}{(\gamma_j + \lambda_i)^2}. \qquad \text{(B-8c)}$$

Equation (B-7) yields a time domain solution

$$n(t) = \Lambda^* \int_0^t G(t - \tau)Q(\tau)d\tau. \tag{B-9}$$

Now consider a pulsed source of the form

$$Q(t) = Q \sum_{\mu=0}^{M} \delta(t - \mu T) \tag{B-10}$$

where Q is the number of neutrons per burst and T is the period of pulsing. After m + 1 pulses, Eq. (B-9) may be written as

$$n_{m+1}(t) = \Lambda^* \int_0^t G(t - \tau)Q \sum_{\mu=0}^{m} \delta(\tau - \mu T)d\tau \tag{B-11}$$

$$= \Lambda^* Q \int_0^t \sum_{j=0}^{\ell} A_j e^{\gamma_j(t-\tau)} \sum_{\mu=0}^{m} \delta(\tau - \mu T)d\tau.$$

By expanding in a series and factoring $A_j e^{\gamma_j t}$

$$n_{m+1}(t) = \Lambda^* Q \sum_{j=0}^{\ell} A_j e^{\gamma_j t} \left\{1 + e^{-\gamma_j T} + e^{-\gamma_j 2T} + \ldots + e^{-\gamma_j mT}\right\}. \tag{B-12}$$

Then note that

$$\frac{1 - e^{-\gamma_j(m+1)T}}{1 - e^{-\gamma_j T}} = 1 + e^{-\gamma_j T} + e^{-\gamma_j 2T} + \ldots + e^{-\gamma_j mT}.$$

Hence the neutron density may be written as

$$n_{m+1}(t) = \Lambda^* Q \sum_{j=0}^{\ell} A_j e^{\gamma_j t} \frac{1 - e^{-\gamma_j(m+1)T}}{1 - e^{-\gamma_j T}}. \tag{B-13}$$

Gozani then introduces the multichannel time, θ, where $\theta = t - mT$ and $0 \leq \theta \leq T$. For convenience, the time reference is shifted and expressed in the multichannel time, substituting θ into Eq. (B-13) yields

$$n_{m+1}(\theta) = \Lambda^* Q \sum_{j=0}^{\ell} A_j e^{\gamma_j \theta} \frac{e^{\gamma_j mT} - e^{-\gamma_j T}}{1 - e^{-\gamma_j T}} . \qquad \text{(B-14)}$$

To improve the statistical precision, the neutron density is allowed to accumulate with repetitive pulses. The neutron density given in Eq. (B-14) can be expressed as a summation for the series of pulses as follows

$$n(\theta) = \sum_{m=0}^{M-1} \Lambda^* Q \sum_{j=0}^{\ell} A_j e^{\gamma_j \theta} \frac{e^{\gamma_j mT} - e^{-\gamma_j T}}{1 - e^{-\gamma_j T}} . \qquad \text{(B-15)}$$

By changing the order of summation, expanding in an infinite series, and collecting positive and negative terms, the solution for $n(\theta)$ is thus

$$n(\theta) = \Lambda^* Q \sum_{j=0}^{\ell} A_j \left\{ \frac{M}{1 - e^{\gamma_j T}} + \frac{1 - e^{\gamma_j}}{2 - e^{\gamma_j T} - e^{-\gamma_j T}} \right\} e^{\gamma_j \theta} . \qquad \text{(B-16)}$$

Now, accurate approximations can be made which will lead to the desired result. Since the decay constant of the prompt fundamental mode $|\gamma_0|$ is much larger than $|\gamma_j|$ for the delayed neutrons, the following approximations can be made: $|\gamma_0|\, T \gg 1$, $|\gamma_j|\, T \ll 1$, and $M \gg 1$. Equation (B-16) can be written as

$$n(\theta) = \Lambda^* Q \left\{ A_0 \frac{M}{1 - e^{\gamma_0 T}} + \frac{A_0 (1 - e^{\gamma_0 MT})}{2 - e^{\gamma_0 T} - e^{-\gamma_0 T}} \right\} e^{\gamma_0 \theta} \qquad \text{(B-17)}$$

$$+ \Lambda^* Q \sum_{j=1}^{\ell} A_j \left\{ \frac{M}{1 - e^{\gamma_j T}} + \frac{1 - e^{\gamma_j MT}}{2 - e^{\gamma_j T} - e^{-\gamma_j T}} \right\} e^{\gamma_j \theta} .$$

Applying the approximation that $|\gamma_0 MT| \gg |$ and $M \gg 1$ the first term of Eq. (B-17) can be approximated so that

$$n_{pr_0}(\theta) = \Lambda^* QM \frac{A_0 e^{\gamma_0 \theta}}{1 - e^{\gamma_0 T}} . \qquad \text{(B-18)}$$

Considering the term

$$\frac{Me^{\gamma_j\theta}}{1 - e^{\gamma_j T}}$$

in the second part of Eq. (B-17), write $1 - e^{\gamma_j T}$ as

$$1 - \left[1 - \gamma_j T + \frac{(\gamma_j T)^2}{2}\right]$$

and

$$e^{\gamma_j\theta} = 1 + \gamma_j\theta.$$

Then dividing and neglecting second order terms yields

$$n_{pr_j}(\theta) = \Lambda^* Q \sum_{j=1}^{\ell} \frac{A_j M}{-\gamma_j T}\left(1 - \gamma_j\theta - \frac{\gamma_j T}{2}\right) \qquad \text{(B-19)}$$

which can be rearranged becoming

$$n_{pr_j}(\theta) = \Lambda^* QM\left\{\frac{1}{T}\sum_{j=1}^{\ell}\frac{A_j}{-\gamma_j}\left[1 + \left(\frac{T}{2} - \theta\right)\frac{\sum_{j=1}^{\ell} A_j}{\sum_{j=1}^{\ell}\frac{A_j}{-\gamma_j}}\right]\right\}. \qquad \text{(B-20)}$$

The second part of the second term in Eq. (B-17) which is the delayed neutron contribution, following a similar procedure, can be written as

$$n_d(\theta) = \frac{-\Lambda^* Q}{T^2}\left\{\sum_{j=1}^{\ell}\frac{A_j}{\gamma_j^2}\left(1 - e^{\gamma_j MT}\right) + \sum_{j=1}^{\ell}\frac{A_j}{\gamma_j}\left(1 - e^{\gamma_j MT}\right)\theta\right\}. \qquad \text{(B-21)}$$

The second term in Eq. (B-21) is small, so assume that $1 - e^{\gamma_j MT} \approx 1$. Gozani also shows that

$$\sum_{j=1}^{\ell}\frac{A_j}{\gamma_j} = \frac{1}{-\rho(\rho - 1)}.$$

Therefore, Eq. (B-21) can be written as

$$n_d(\theta) = \frac{\Lambda^* Q}{T^2}\left\{\sum_{j=1}^{\ell}\frac{A_j}{\gamma_j^2}\left(1 - e^{\gamma_j MT}\right) - \frac{\theta}{\rho(\rho - 1)}\right\}. \qquad \text{(B-22)}$$

Combining Eqs. (B-18), (B-21) and (B-22) to obtain the total neutron response, then rearranging terms yields

$$n(\theta) = \Lambda^* QM\left\{\frac{A_0 e^{\gamma_0\theta}}{1 - e^{\gamma_0 T}} + \frac{1}{T}\sum_{j=1}^{\ell}\frac{A_j}{-\gamma_j}\left[1 + \left(\frac{T}{2} - \theta\right)\frac{\sum_{j=1}^{\ell} A_j}{\sum_{j=1}^{\ell}\frac{A_j}{-\gamma_j}} - D(MT, \rho)\right]\right\} \qquad \text{(B-23a)}$$

where

$$D(MT, \rho) = \frac{1}{MT}\frac{\left\{\sum_{j=1}^{\ell}\frac{A_j}{\gamma_j^2}\left(1 - e^{\gamma_j MT}\right) - \frac{\theta}{\rho(\rho - 1)}\right\}}{\sum_{j=1}^{\ell}\frac{A_j}{-\gamma_j}}. \qquad \text{(B-23b)}$$

The first term in Eq. (B-23) represents the prompt response, and the second term is descriptive of the delayed neutrons. For the conditions of the pulsed experiment, the second term decays slowly and is almost constant with θ.

Equation (B-23) is now used to derive an expression for reactivity. First, rewrite as

$$n(\theta) = \Lambda^* QM\left\{\frac{A_0 e^{\gamma_0\theta}}{1 - e^{\gamma_0 T}} + \frac{1}{T}\sum_{j=1}^{\ell}\frac{A_j}{-\gamma_j} C_d\right\}. \qquad \text{(B-24)}$$

In Eq. (B-24) C_d is a small correction factor the admixture of prompt and delayed neutrons eigenvalues. Note that $N(\theta) = N_{pr} + N_d$ where

$$N_{pr} = \frac{\Lambda^* QMA_0 e^{\gamma_0\theta}}{1 - e^{\gamma_0 T}} \qquad \text{(B-25)}$$

and

$$N_d = \frac{1}{T} \Lambda^* QM \sum_{j=1}^{\ell} \frac{A_j}{-\gamma_j} C_d \tag{B-26}$$

At $\theta = 0$, Eq. (B-25) becomes

$$N_{pr}(0) = \frac{\Lambda^* QM \gamma_0}{(\rho - 1)(1 - e^{\gamma_0 T})} \tag{B-27}$$

and Eq. (B-26) becomes

$$N_d = \frac{1}{T} \frac{1}{\rho(\rho - 1)} C_d \Lambda^* QM \tag{B-28}$$

where

$$\frac{A_j}{-\gamma_j} \cong \frac{1}{\rho(\rho - 1)} .$$

Dividing Eq. (B-27) by Eq. (B-26), then solving for reactivity yields

$$\rho = \frac{N_{pr}(0)(1 - e^{\gamma_0 T})}{T N_d \gamma_0} C_d . \tag{B-29}$$

Equation (B-29) is the desired result noting that $T \times N_d$ is the area under the constant delayed curve and

$$\frac{N_{pr}(0)(1 - e^{\gamma_0 T})}{\gamma_0}$$

is the negative of the area under the extrapolated fundamental prompt decay curve.

$$\int_0^T N_{pr}(0) e^{\gamma_0 \theta} d\theta = \frac{N_{pr}(0)(e^{\gamma_0 T} - 1)}{\gamma_0} . \tag{B-30}$$

Thus, Eq. (B-29) is often given as

$$\rho_{\$} = \frac{\text{Prompt area}}{\text{Delayed area}} \times C_d \ . \qquad \text{(B-31)}$$

In Eq. (B-31) C_d is usually small on the order of several per cent.

XII. APPENDIX C

GRIPE II was originally written by Kaufman [14] in Fortran IV for analysis of data from pulsed-neutron experiments. This program has been made operational on the ISU IBM-360 computer with some minor modifications [20]. The description of GRIPE II presented here follows that given by Kaufman [14]. For convenience in this section the subscript on alpha denoting fundamental mode is omitted.

For a subcritical assembly GRIPE II assumes that the data satisfies the following conditions. $N(t) = N_p(t) + N_d + B$ where $N_p(t)$ is the prompt neutron response as a function of time, N_d is the constant delayed neutron background and B is a constant reactor background. It is necessary that $N_p(t) = N_a \exp(-\alpha t)$ after some time interval τ where τ is less than $0.7 \times (\beta/\Lambda)$ for the solution routine to converge.

For each experiment two sets of data are needed. One is the background data B obtained when the neutron pulse source is inoperative. The second set of data is the reactor response to the pulsed source as recorded by the time base analyzer. A sufficient number of pulses is needed to obtain statistically meaningful data. This second set of data also contains the delayed neutrons as the reactor returns to equilibrium after pulsing ceases.

The program operates on the data in the following manner. The data are scanned for missing points, and these missing points are estimated. Next, a resolution correction is performed with the following formula,

$$N_T = N_o/(1 - t_r N_o) \qquad (C\text{-}1)$$

which is descriptive of a non-paralyzable system. Kaufman points out that the use of this equation assumes that the output of the neutron generator is constant. The count rate is determined for each channel and the correction is made.

After the resolution correction has been made, the program calculates statistical estimates for the constants $(N_d + B)$, B, and N_d. Each data set is assumed to be a statistical variation about a constant value after a channel number called the "first point of the constant portion of the data", FC. For example, the FC point could be considered channel 2 for background data, or channel 375 for pulsed data. The "last channel of the constant portion of the data", LC, must also be supplied. Then an estimate of the constant value B, $\bar{B}$ is calculated by

$$\bar{B} = \sum_{i=FC}^{LC} \left[\sum_{j=1}^{J} N_{ij} \right] / (LC - FC + 1) \qquad (C\text{-}2)$$

and the standard deviation by

$$S_1^2 = \sum_{i=FC}^{LC} \left[\sum_{j=1}^{J} N_{ij} - \bar{B} \right]^2 / (LC - FC). \qquad (C\text{-}3)$$

The variance of B is then calculated by

$$\sigma_B^2 = S_1^2/(LC - FC + 1). \qquad (C\text{-}4)$$

At this point the $\bar{B}$ is made compatible with the pulsed data to correct for any difference in gate width, or differences in the number of sweeps. The corrected background is

$$B_e = \overline{B} \times (GW_e/GW_b) \qquad (C\text{-}5)$$

where GW_e is the effective gate width and GW_b is the actual gate width. For example, if the number of sweeps in the pulsed experiment is 25000, the number of background sweeps is 12500, and the actual gate GW is 0.0001 sec, then the effective gate width should be changed to 0.0002 sec.[a]

When processing the pulsed data GRIPE II uses Eq. (C-2) to find $\overline{N_d + B}$ except that FC is a channel number in the constant region of the pulsed data. $\overline{N_d + B}$ is then substituted for $\overline{B}$ in Eq. (C-3) to determine the variance, S_2 for the $\overline{N_d + B}$ measurement. It is desirable to make (LC - FC) as large as possible to reduce the variance, but this is difficult to do. The program performs a search by decreasing FC by ten channels then recomputing $\overline{N_d + B}$ and S_2. When the new standard deviation is 1.005 times greater than the previous value, the previous values are assumed best. In this way, the search finds the best value of $\overline{N_d + B}$ in the sense that (LC - FC) is the largest for which the standard deviation of the intermediate data points increased by no more than 0.5 per cent of the initial value. At this time an estimate of $\overline{(N_d + B)}$ is obtained and the variance defined as

$$\sigma^2_{\overline{N_d+B}} = (S_2)^2/(LC - FC + 1). \qquad (C\text{-}6)$$

N_d is then calculated by

---

[a] No provision has been made for propagation of errors in this case so that $S1_e = S1 \times (GW_e/GW_b)$ and $\sigma^2_{Be} = \sigma^2_B(GW_e/GW_b)^2$. Best results are obtained with $GW_e = GW_b$.

$$N_d = \overline{N_d + B} - \overline{B} \qquad (C\text{-}7)$$

with its variance defined as

$$\sigma^2_{N_d} = \sigma^2_B + \sigma^2_{\overline{N_d+B}} \; . \qquad (C\text{-}8)$$

Since the input data for the pulsed experiment was assumed to be of the form $N(t) = N_p(t) + N_d + B$, GRIPE II isolates the prompt decay by subtracting the computed value for $\overline{N_d + B}$ from each point of $N(t)$. The prompt data is then represented by $N_p(Ti) + E(Ti)$ where $E(Ti)$ is the difference between $\overline{(N_d + B)}$ and the statistically varying estimate of $(N_d + B)$ at Ti.

In order to obtain values which are least influenced by $E(Ti)$, GRIPE II assumes that the data in the latter channels were truly descriptive of a constant. Then all values of $N_p(Ti)$ which are greater than some standard deviation multiplier, SM, times S_2 will be descriptive of $N_p(t)$. For example, if SM is 10.0, only values of $N_p(Ti)$ which are greater than $10.0 \times S_2$ will be descriptive of $N_p(t)$; thus, 99.9 per cent of the time no $E(Ti)$ will constitute more than 30 per cent of any value of $N_p(Ti)$. The value of SM is specified in the data input. When SM is large, the number of points used in determining α will be small, but the influence of $E(Ti)$ is also small. Conversely, if the value of SM is small, the number of points used in determining $N_p(t)$ will be large. The value of 10.0 for SM seems to give optimum results which balance the greatest number of points with the minimum influence of $E(Ti)$. The value of $SM \times S_2$ determines the last channel number for which $N_p(Ti) > SM \times S_2$. This channel is considered to be the last point defining an exponential decay.

The next step is the determination of α and $N_p(0)$. In order to do this, GRIPE II uses an initial guess for a channel number after which $N_p(t)$ is described by $N_p(0)\exp[-\alpha t]$. If the channel number was selected properly, the data in the form $\ln[N_p(Ti)]$ should fit a linear model. This form is $\ln[N_p(Ti)] = \ln N_p(0) - \alpha Ti$. In the first iteration, GRIPE II assumes that the previous condition is satisfied and calculates the values of $\ln N_p(0)$ and α which provide the best linear fit to the data $\ln[N_p(Ti)]$ in a weighted least-squares sense.

Each of the squares of the residuals in a least-squares fit is weighted by a number W(Ti) which is calculated by

$$W(Ti) = [N_p(Ti)]^2/[N_p(Ti) + N_d + B + (S_2)^2]. \qquad (C\text{-}9)$$

This weighting factor has been selected as equal to the reciprocal of the square of the expected error in $\ln[N_p(Ti)]$. Kaufman points out that such a selection ensures that each residual is treated as a statistical variation about the model postulated rather than permitting the larger values of the data to disproportionately influence the data fit. From this fit, $\ln(N_p(0))$, the variance of each, and the covariance are calculated. The expected error in $\ln[N_p(Ti)]$ is calculated as

$$\delta N_p(Ti) = \sqrt{\left[\sum_{FE=1}^{LE} N_{TE}(Ti) - \overline{N_o + B}\right]^2 + \left[\overline{\delta(N_o + B)}\right]^2}. \qquad (C\text{-}10)$$

The iteration procedure for α is used to eliminate some of the experimental difficulties. Three factors are considered to be the most probable causes of error. First, if the estimate of channel FE was

too small, the early channels considered in the fit would not have reached an exponential decay. Second, variations in the neutron generator yield would cause variations in the early channels. Third, if SM was not appropriate, the data in the channels around LE would be significantly influenced by the error function E(Ti). Since these factors have an influence on the fit, the iterative scheme used in GRIPE II is to omit front and back channels from FE and LE. Another fit is calculated as before on the smaller number of channels. At this point, two tests are made to determine if the value of α_2 in the second iteration is better than the first. If α_1 is the best, then the $|\alpha_1 - \alpha_2|$ is most probably less than σ_{α_1}. Since fewer data points were used, it is also most probable that $\sigma^2_{\alpha_2}$ is greater than $\sigma^2_{\alpha_1}$. However, if α_2 is a better fit to the linear model it is most probable that $\sigma^2_{\alpha_2}$ will be less than $\sigma^2_{\alpha_1}$ and that $|\alpha_2 - \alpha_1|$ will be larger than σ_{α_1}. If $|\alpha_2 - \alpha_1|$ is less than σ_{α_1}, and if $\sigma^2_{\alpha_2} > \sigma^2_{\alpha_1}$, the program assumes that the first α, α_1 is descriptive of an exponential decay. However, if either test is not satisfied, the data set is reduced again by the specified number of channels from the first channel and the last channel of the fit. Another test has been added to insure that the decay constant is converging. This test consists of continuing the iteration for α until the variation in χ^2 is less than a specified deviation. The formulation of this test added by Moen [21] to GRIPE II is

$$\left(\frac{\chi^2}{N} - 1\right) \leq \text{SDM}\ \sigma_{\chi^2} \qquad \text{(C-11)}$$

where N is the number of points used in the fit, and SDM is the standard deviation multiplier. Chi squared is determined by

$$\chi^2 = \sum_{i=FE}^{LE} \frac{[N_p(Ti) - N_p(0)\exp(-\alpha Ti)]^2}{N_p(0)\exp(-\alpha Ti) + N_d + B} \quad . \tag{C-12}$$

After suitable values for α, N_d, $\ln N_p(0)$, $N_p(t)$, and their variances are determined, the reactivity calculations are made. First, the extrapolated area-ratio method is calculated by the expression

$$\rho(\$)_{GOZ} = \frac{R \times N_p(0)}{\alpha \times N_d \times K} \tag{C-13}$$

where R is the effective pulse rate in pulses per sec, $N_p(0) = \exp[\ln N_p(0)]$, α is the calculated decay constant, N_d the delayed neutron constant, and K is the kinetic distortion factor. Then an estimate of (β/Λ) is made from

$$(\beta/\Lambda)_{GOZ} = \frac{\alpha}{1 + \rho(\$)_{GOZ}} \quad . \tag{C-14}$$

The variance of reactivity is computed from

$$\sigma^2_{\rho_{GOZ}} = \rho(\$)^2_{GOZ}\left[\frac{\sigma^2_\alpha}{(\alpha)^2} + \frac{\sigma^2_{N_d}}{(N_d)^2} + \frac{\sigma^2_{N_p(0)}}{N_p(0)} - 2\,\frac{\sigma_{\alpha,\,N_p(0)}}{[N_p(0)][\alpha]}\right] \tag{C-15}$$

where the variance $\sigma^2_{N_p(0)} = N_p(0)^2\sigma^2_{\ln(N_p(0))}$, and the covariance of α and $N_p(0)$, $\sigma_{\alpha,N_p(0)} = N_p(0) \times \sigma_{\alpha,m(N_p(0))}$.

The variance for (β/Λ) is calculated by the following expression

$$\sigma^2_{(\beta/\Lambda)} = \left(\frac{\beta}{\Lambda}\right)^2\left[\frac{\sigma^2_\rho}{(1+\rho)^2} + \frac{\sigma^2_\alpha}{(\alpha)^2} - \frac{2\rho}{\alpha(1+\rho)}\left(\frac{\sigma_{\alpha,N_p(0)}}{N_p(0)} - \frac{\sigma^2_\alpha}{\alpha}\right)\right] . \tag{C-16}$$

The next step is the reactivity calculation by the Garelis-Russell method,

$$\rho(\$)_{G\text{-}R} = \left(\frac{\alpha}{\beta/\Lambda}\right) - 1 \qquad \text{(C-17)}$$

where β/Λ is the root of the following equation

$$\int_0^{\infty} N_p(t)\exp[(\beta/\Lambda)t]dt - \int_0^{\infty} N_p(t)dt = \frac{N_d}{R} K. \qquad \text{(C-18)}$$

The integrals are taken to ∞ instead of 1/R because the contribution to the integrals after 1/R is approximately zero. The solution of Eq. (C-18) is done with a direct approach rather than an iterative technique because of the weighting influence of $\exp(\beta/\Lambda)t$ on the statistically poor later channels. The direct approach should be more accurate, but requires that the time at the first exponential be less than 0.7 β/Λ. This restriction appears to be insignificant in the UTR-10 reactor. The restriction is a result of the expansion of the $\exp(\beta/\Lambda\ t_{FE})$ in a Maclaurin series where sixth order and higher terms are neglected.

The resulting sixth order equation is solved for β/Λ

$$- \left(\frac{\beta}{\Lambda}\right)^6\left[\frac{1}{120}\int_0^\tau F(t)t^5dt\right] + \left(\frac{\beta}{\Lambda}\right)^5\left[\frac{\alpha}{120}\int_0^\tau F(t)t^5dt - \frac{1}{24}\right.$$

$$\left.\int_0^\tau F(t)t^4dt + \frac{N_p(0)\tau^5\exp(-\alpha\tau)}{120}\right] + \left(\frac{\beta}{\Lambda}\right)^4\left[\frac{\alpha}{24}\int_0^\tau F(t)t^4dt - \frac{1}{\sigma}\right.$$

$$\left.\int_0^\tau F(t)t^3dt + \frac{N_p(0)\tau^4\exp(\alpha\tau)}{24}\right] + \left(\frac{\beta}{\Lambda}\right)^3\left[\frac{\alpha}{6}\int_0^\tau F(t)t^3dt - \frac{1}{2}\right.$$

$$\left.\int_0^\tau F(t)t^2dt + \frac{N_p(0)\tau^3\exp(-\alpha\tau)}{6}\right] + \left(\frac{\beta}{\Lambda}\right)^2\left[\frac{\alpha}{2}\int_0^\tau F(t)t^2dt\right.$$

$$\left.- \int_0^\tau F(t)tdt + \frac{N_p(0)\tau^2\exp(-\alpha\tau)}{2}\right] + \left(\frac{\beta}{\Lambda}\right)^2\left[\alpha\int_0^\tau F(t)tdt\right.$$

$$\left.- N_a\tau\exp(-\alpha\tau) + \frac{N_p(0)\exp(-\alpha\tau)}{\alpha} + \frac{N_dK}{R}\right] - \left[\frac{N_dK\alpha}{R}\right] = 0. \qquad \text{(C-19)}$$

The value used to calculate reactivity is one of the six roots of Eq. (C-19). A range is supplied to allow GRIPE II to choose the proper root. For the UTR-10, a range of 30 sec^{-1} to 200 sec^{-1} was used, and only one root was found. The uncertainty in β/Λ is determined from

$$\sigma^2_{\beta/\Lambda} = \left(\frac{\partial\,\beta/\Lambda}{\partial\alpha}\right)^2\sigma^2_\alpha + \left(\frac{\partial\,\beta/\Lambda}{\partial N_d}\right)^2\sigma^2_{N_d} + \left(\frac{\partial(\beta/\Lambda)}{\partial\,N_p(0)}\right)^2\sigma^2_{N_p(0)}$$

$$+ 2\left(\frac{\partial\,\beta/\Lambda)}{\partial\alpha}\right)\left(\frac{\partial\,\beta/\Lambda}{\partial\,N_p(0)}\right)\sigma_{\alpha,N_p(0)} \qquad \text{(C-20)}$$

where the other variances have been determined. Then the variance of the reactivity is calculated from the equation

$$\sigma^2_\rho = \left(\frac{\alpha^2}{\beta/\Lambda}\right)^2\left\{\frac{\sigma^2_\alpha}{\alpha^2} + \frac{\sigma^2_{\beta/\Lambda}}{(\beta/\Lambda)^2} - \frac{2}{\alpha\,\beta/\Lambda}\left[\left(\frac{\partial\,\beta/\Lambda}{\partial\,N_p(0)}\right)\sigma_{\alpha,N_p(0)} + \left(\frac{\partial\,\beta/\Lambda}{\partial\alpha}\right)\sigma^2_\alpha\right]\right\}. \qquad \text{(C-21)}$$

Although not covered in the GRIPE II manual, Kaufman has also added a step in the program which calculates Sjöstrand's area-ratio reactivity from the known quantities in the program. This reactivity also appears in the output analysis page.

Table C-I indicates the card number, symbol, control function and format[a] of the cards used in program control. One set of these cards precedes the entire data deck. The cards in Table C-II are used to indicate the properties of each data deck. The four cards described in this table precede each data deck.

---

[a]Care must be exercised in use of proper formats and note that all I formats are right justified.

Table C-I. Program control cards

Card No.	Location (column)	Symbol	Control function	Format
1	1-5	—	The number of decks to be processed. For example, of one background and one pulsed run are processed, the number 2 is used.	I-5
2	1-20	β/Λ	A conservatively small estimate of β/Λ.	6x E14.7
	21-40	β/Λ	A conservatively small estimate of β/Λ.	6x E14.7
3	1-2	Punch control	Enter a 0 and no cards are punched; enter 1 for a set of punched cards containing the prompt neutron data corrected for dead time and background.	I-2
	3-4	Print control	Enter 0 for no print, and 1 for a print out containing the corrected prompt neutron data which is the same as the punched data.	I-2
	5-6	Reactivity control	Enter 0 and reactivity will be calculated, enter 1 in column six and reactivity step is skipped.	I-2
	7-17	SDM	Standard deviation multiplier for χ^2 test on α convergence, if equal to 2.0 the convergence parameter is $\pm 2 \sigma_{\chi^2}$ in Eq. (C-11).	F10.0

Table C-II. Data set control cards

Card No.	Location (column)	Symbol	Control function	Format
1	1-5	—	Data type 0 — Reactor pulsed at critical 1 — Reactor background 2 — Reactor pulsed when sub-critical	I-5
	6-10[a]		Plot control, enter 0 for no plot.	I-5
	11-15	FE	Number of channels corresponding to initial guess for time at which exponential decay time is observed. Must be ≥ 1.	I-5
	16-20	FC	The channel past which the data is "known" to be a constant. FC must be > 12 for pulsed data.	I-5
	21-25	LC	The last channel for which the data are constant.	I-5
	26-30	FO	The number of channels omitted from FE in the successive iterations for α.	I-5
	31-35	LO	The number of channels omitted from the last of the data set in successive iterations for α.	I-5
	36-45	SM	Multiplier of S_2 to be used in defining LE, the last data point defining exponential decay.	E 10.5
	46-55	GW_e	This is the effective gate width of the background data. (Used only for type 1 data.)	E 10.5

[a]Plotting section has not been converted to ISU IBM 360.

Table C-II. (Continued)

Card No.	Location (column)	Symbol	Control function	Format
2	1-5	I	Number of points in a data set (generally the number of analyzer channels). Must be $\leq$ 512.	F-5
	6-15	PT	For background data the number of analyzer sweeps. For pulsed data, the number of pulses.	E 10.5
	16-25	RT	Resolving time of the counting system expressed in units of sec.	E 10.5
	26-35	TB	Analyzer time base in sec.	E 10.5
	36-45	R	Effective pulse rate which is equal to the actual pulse rate x the number of analyzer sweeps between pulses.	E 10.5
	46-55	GW_b or GW_p	Analyzer gate width.	E 10.5
	56-65	K	Kinetic distortion multiplier for standard forms K = 1.0.	E 10.5
3	3-80		Problem or data set title.	2x,13A6
4	1-12		Plotting label X axis.	2A6
	13-20		Blank.	8x
	21-32		Plotting label Y axis. (Blank card used.)	2A6

XIII. APPENDIX D

To help future investigators with equipment adjustment, a summary of the instrument control settings is presented in this appendix.

Instrument	Control function	Dial position
RIDL model 3412B analyzer	Store in	0-399
	Horizontal Scale	400
	Cycle Mode	Off
	Reset Mode	External
	Store Mode	Add
	Read Mode	Display during data accumulation Serial during typewriter output
	Master	Store during data accumulation Wait when changing dial position Read for data output
	Toggel Switches Positions	RIDL time Live time Auto transfer-off Non-dest. Time mode
	Amplifier	Not used

Instrument	Control function	Dial position
RIDL Timer	Multiplier	1
	Channel Width	100 μs
	Auto Stop	Off
	Function	Auto Read Out
	Region of interest	1
	Cycle Counter	1
	Cycle Counter Multiplier	Off
	Read Out	Typewriter
	Address	Out
Fluke High Voltage Supply Model 405B (Both supplies)	Voltage	1300 volts
	Polarity	Pos.
D.C. Supply to Trigger Circuit		12-15 volts
ORTEC Model 410 Multimode Amplifier	Input polarity	Neg.
	Fine Gain	1.0
	Integration	Out
	Input Attenuator	1
	Course Gain	3
	Differentiation	1^{st} 0.1 2^{nd} 0.1
	Output	Bipolar

Instrument	Control function	Dial position
Discriminator Mechtronics Model 605	Input-Output	#2
	Threshold	#2 6.6
Scaler/Timer ALRR 003 AEC #15741	Mode	SCA
	Preset	Select
	Polarity	Neg.
	Control	Master
Scaler ALRR 002 AEC #15687	Polarity	Neg.
	Control	Internal
Monitor Circuit Canberra Amplifier Model 816	Mode	Bi
	Input	Neg.
	Course Gain	8
	Fine Gain	4.5
Canberra Discriminator Model 830	Baseline	2.9
	Window Width	Open
Scaler ALRR 002 AEC #15688	Polarity	Pos.
	Control	Ext
	Gate	Scaler/Timer
Kaman Nuclear Neutron Generator Control Console	High Voltage	3.1 – 3.4 KV
	Pressure	Auto 3.5 – 10.0
	Pulse Selector	Remote
	Pulse Mode	Single/Remote